Report

Neuron

Linking Electrical Stimulation of Human Primary Visual Cortex, Size of Affected Cortical Area, Neuronal Responses, and Subjective Experience

Highlights

- Electrical brain stimulation in patients with electrodes in V1 elicited phosphenes
- Phosphenes matched the electrode receptive field measured with broadband potentials
- Phosphene size increased systematically with eccentricity and amount of charge
- Cortical area activated increased with the amount of charge but not eccentricity

Authors

Jonathan Winawer, Josef Parvizi

Correspondence

jonathan.winawer@nyu.edu (J.W.), parvizi@stanford.edu (J.P.)

In Brief

We quantified the area of cortical tissue activated by electrical brain stimulation in human patients. The location of phosphenes evoked by stimulating primary visual cortex matched the receptive field of the cortical site measured with broadband field potentials.

Winawer & Parvizi, 2016, Neuron *92*, 1–7
December 21, 2016
http://dx.doi.org/10.1016/j.neuron.2016.11.008

CellPress

Please cite this article in press as: Winawer and Parvizi, Linking Electrical Stimulation of Human Primary Visual Cortex, Size of Affected Cortical Area, Neuronal Responses, and Subjective Experience, Neuron (2016), http://dx.doi.org/10.1016/j.neuron.2016.11.008

Neuron
Report

Linking Electrical Stimulation of Human Primary Visual Cortex, Size of Affected Cortical Area, Neuronal Responses, and Subjective Experience

Jonathan Winawer[1,3,4,*] and Josef Parvizi[2,3,*]
[1]New York University, New York, NY 10003, USA
[2]Stanford University, Stanford, CA 94305, USA
[3]Stanford Human Intracranial Cognitive Electrophysiology Program (SHICEP), Stanford, CA 94305, USA
[4]Lead Contact
*Correspondence: jonathan.winawer@nyu.edu (J.W.), parvizi@stanford.edu (J.P.)
http://dx.doi.org/10.1016/j.neuron.2016.11.008

SUMMARY

Electrical brain stimulation (EBS) complements neural measurements by probing the causal relationship between brain and perception, cognition, and action. Many fundamental questions about EBS remain unanswered, including the spatial extent of cortex responsive to stimulation, and the relationship between the circuitry engaged by EBS and the types of neural responses elicited by sensory stimulation. Here, we measured neural responses and the effects of EBS in primary visual cortex in four patients implanted with intracranial electrodes. Using stimulation, behavior, and retinotopic mapping, we show the relationship between the size of affected cortical area and the magnitude of electrical charge. Furthermore, we show that the spatial location of electrically induced visual sensations is matched to the receptive field of the cortical site measured with broadband field potentials, and less so with event related potentials. Together, these findings broaden our knowledge about the mechanism of EBS and the neuromodulation of the human brain.

INTRODUCTION

Focal stimulation of human cerebral cortex has long been known to elicit (Bartholow, 1874; Brindley and Lewin, 1968; Dobelle and Mladejovsky, 1974; Penfield and Perot, 1963), or interfere with (Ojemann et al., 1989), specific and complex behaviors and experiences, making it a powerful tool for investigating the cortical basis for perception, thought, and behavior. EBS studies in nonhuman primates have greatly advanced our understanding of sensory processing and perceptual decision making (Cohen and Newsome, 2004; Salzman et al., 1990), and studies in other mammalian brains have begun to uncover the fine-grained effects of EBS (Histed et al., 2009).

While past studies in animals have yielded important knowledge about microstimulation of the brain (Tehovnik and Slocum, 2007), much remains to be known about the effect of EBS in the human brain. Typical animal and human EBS studies differ 1,000-fold in electrode diameter, impedance, and electrical current. Thus, the generalizability from animal models to clinical neuromodulation is unknown (Borchers et al., 2011).

To study the effect of EBS on human cerebral cortex, we took advantage of the topographic organization of primary visual cortex (V1) to (1) quantify the size of affected cortical area as a function of electrical charge using a novel, model-based approach, and (2) assess how the circuitry engaged by EBS relates to neural signals elicited by sensory stimulation.

Four patients with focal epilepsy were implanted with intracranial electrodes for clinical monitoring (Table S1). EBS was applied to pre-selected V1 electrodes (Figures 1A and 1B), outside the patients' pathological zones, using square-wave pulses with varying frequency (5–100 Hz), pulse width (200–1,000 μs), amplitude (0.2–5 mA), and duration (0.2–1 s) (Table S2). EBS produced localized visual sensations (phosphenes) (Foerster, 1929), quantified in two ways: subjects outlined the phosphene on a computer screen following stimulation (sites 1–5) and rated the intensity of the phosphene on a 0–10 scale (sites 2, 3, and 5). There were 0 false positives and only 4 false negatives (13 shams stimulations, 102 trials; Table S2). In a control experiment, we confirmed the reliability of each subject's tracing (Figure S2).

RESULTS

Separating ECoG Signals into Component Responses

In each subject, we recorded intracranial electrophysiological signals (ECoG) from the stimulated site. The field potential measured by ECoG shows a response when the stimulus is in the site's population receptive field ("pRF" [Dumoulin and Wandell, 2008; Yoshor et al., 2007]). Since the ECoG signal sums the responses generated by multiple types of neural sources (Buzsáki et al., 2012), we separated the visually driven ECoG response into two complementary components: the steady-state visual-evoked potential, which is time locked to the visual stimulus (Adrian and Matthews, 1934; Norcia et al., 2015), and broadband power, which is a rise in the variance in response to a stimulus (Miller et al., 2014) (Figures 1C and 1D). This rise in variance is superimposed on a power spectrum approximately of the form, $power \propto 1/f^n$, where f is the temporal frequency and n is a constant (Miller et al., 2009; Milstein et al., 2009). This

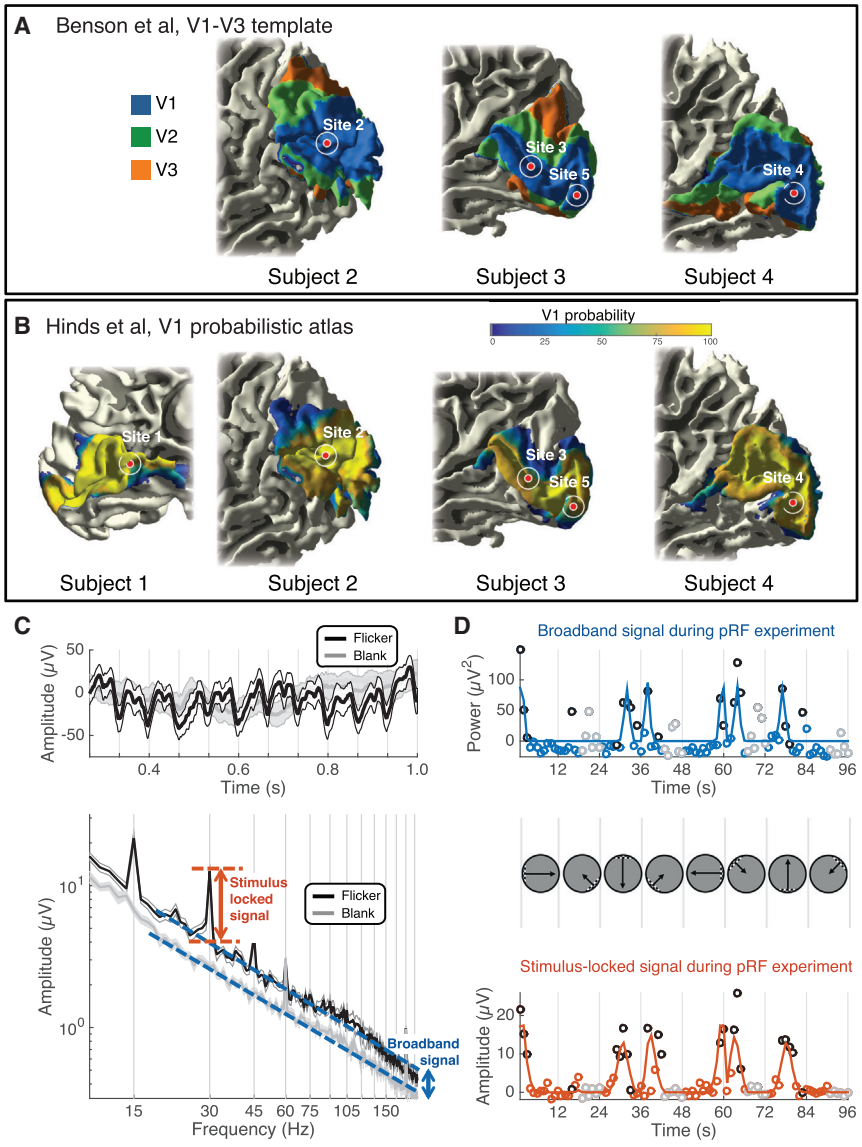

Figure 1. Electrophysiological Signals in V1 Electrodes

(A and B) A template of V1–V3 (Benson et al., 2014; A) and a probabilistic atlas of V1 (Hinds et al., 2008; B) were applied to each subject's T1-weighted anatomical MRI. The electrodes used for EBS are shown as red circles. The white circle indicates positional uncertainty of 5 mm in radius. All electrodes are within the Benson template V1 (the template failed on subject 1 due to poor alignment with the standard anatomical image in FreeSurfer) and high probability areas of the Hinds V1.

(C) Mean time series (top) and amplitude spectra (bottom) from several 1 s epochs during visual mapping experiments from an example V1 electrode (site 2). The traces show data averaged across 24 epochs when the bar stimulus was near the site's pRF (black), or when the stimulus was blank (gray). The shaded region indicates ±1 SEM across 24 epochs. The arrows depict the stimulus locked (orange) and broadband (blue) signals.

(D) The 96 s experiment was summarized with two time series, broadband (upper) and stimulus locked (lower). The trajectory of the bar apertures is shown between the upper and lower plots. Blue and orange lines are pRF model fits to the data, and circles are the data (either broadband or stimulus locked measurement from each epoch). Black and gray circles indicate the 24 epochs summarized in (C) (flicker and blank, respectively). See Figure S1 and Table S1.

constant *n* in our data, computed for the blank stimulus conditions over the range 10–200 Hz was approximately 2.6 (2.9. 2.2, 2.9, 2.4, 2.6; sites 1–5). Prior work has shown that broadband and evoked potentials pool spatial information differently and likely arise from different neuronal population and network activity (Winawer et al., 2013). The broadband signal clearly spans a wide frequency range (10 to 200 Hz; Figure 1C), although in other studies this signal is most evident in the high frequencies and hence is often referred to as "high gamma" or "high frequency broadband" (Canolty et al., 2006; Crone et al., 1998).

Overlap between Phosphenes and ECoG pRFs

The overlap between EBS phosphenes and ECoG pRFs was best for the ECoG broadband response. For each site, separate pRFs were computed from the broadband and stimulus-locked time series (Figures 2A and 2B). The two types of pRFs yielded similar but not identical solutions (Figure 2C). They did not differ substantially in accuracy, with an average variance explained for the five sites of 80.8% for the broadband pRF and 80.5% for the stimulus-locked pRF (Figure 2D, inset, and columns 2 and 3 in Table S3), indicating that models from each component of the ECoG signal provided excellent fits to the corresponding time series.

For sites 1–4, the phosphenes were better matched to the pRFs derived from the broadband time series than the stimulus-locked time series (Figure 2C). For site 5, corresponding to the fovea (<1°), the pRFs were much larger than the phosphenes, likely due to challenges of accurately measuring very small receptive fields near the central fovea (Dougherty et al., 2003). These observations were quantified by computing a measure of overlap, the Dice coefficient, between either the broadband or stimulus-locked pRF for a given site (thresholded to within 2 standard deviations of the Gaussian pRF) and each of the phosphenes drawn by the subjects when that site was stimulated (Figure 2D; Figure S3). For sites 1–4, the overlap coefficient was significantly higher for the broadband pRFs than the stimulus-locked pRFs ($p = 0.020$, 0.000, 0.000, 0.006; tests of bootstrapped means, Table S3). For site 5, the overlap coefficient was significantly higher for the stimulus-locked pRF ($p = 0.000$), though the overlap coefficient was low for both measures (less than 0.03, 5–20 times less than the coefficients for the other 4 channels).

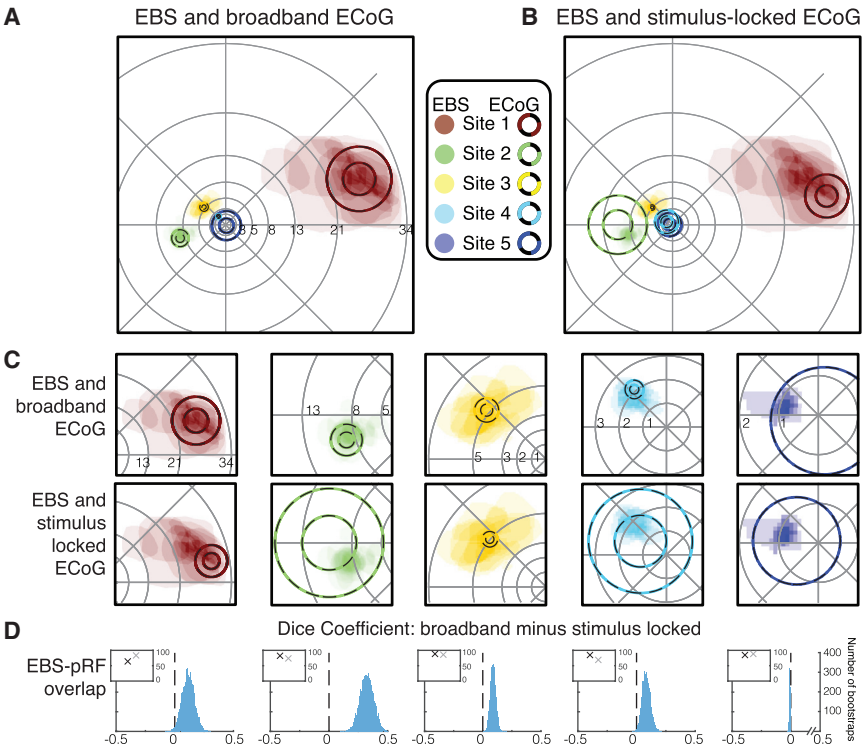

Figure 2. Comparison of Spatial Selectivity between EBS and ECoG

(A) A comparison of pRFs derived from broadband ECoG data (circles, 1- and 2-SD lines) and phosphenes drawn by subjects (shaded regions). The number of phosphenes drawn for the 5 sites was 18, 21, 16, 18, and 9 (Sites 1–5).

(B) Same as (A) except that pRFs are derived from the stimulus-locked ECoG data.

(C) Zoom of the data from (A) (upper plots) and (B) (lower plots).

(D) Each histogram shows the difference in overlap (Dice coefficient) between the phosphenes and broadband pRF versus the phosphenes and stimulus-locked pRFs. A positive number on the x axis means greater overlap between the phosphene and broadband pRF than between the phosphene and stimulus-locked pRF. Histograms were derived by bootstrapping over stimulation trials. For sites 1–4, the overlap with the broadband pRF is greater than with the stimulus-locked pRF (histograms to the right of 0). For site 5, the pRF is very foveal and not accurately estimated by the ECoG data; hence, the overlap coefficient is low for both types of pRFs. Insets show variance explained by the pRF models (black, broadband; gray, stimulus locked). The variance explained is similar for the two types of pRF models. See Figures S2 and S3 and Tables S2 and S3.

Effect of Stimulation Parameters on Size of Phosphenes and Responsive Cortex

Across EBS trials, the phosphenes on average showed a high level of overlap with broadband pRFs measured from the same electrode. The phosphenes, however, were not identical on each trial and tended to be larger on trials with greater electrical charge (Table S2). We took advantage of these trial-to-trial differences to quantify the spatial extent of activated cortex as a function of electrical charge. To do so, we devised a model that relied on the retinotopic map of V1, derived from pre-operative fMRI or by fitting a template to the subject's anatomical MRI (Benson et al., 2014). From the retinotopic map, we know the relationship between locations in the visual field and locations on cortex. The spatial overlap between fMRI, broadband ECoG, and EBS phosphenes (Figures 3A–3C) indicates that it is reasonable to assume that the V1 response near the electrode corresponds to the spatial location of the phosphenes. To quantify the relationship between electrical charge and the size of the cortical area affected by EBS, we projected the subjects' phosphene outlines onto the same subject's V1 map, yielding a measure of cortical area for each EBS trial (Figure 3D). We then asked how the phosphene area in the visual field and the phosphene area projected onto cortex varied with electrical charge.

The relationship between charge and phosphene size in the visual field showed two clear patterns: stimulating with more charge or stimulating more peripheral receptive fields caused larger phosphenes (Figure 4A). The cortical area of phosphenes also increased as a function of charge deposited (Figure 4B) but did not differ systematically as a function of eccentricity. The apparent discrepancy between phosphene size in the visual field and on cortex is reconciled by the pattern of cortical magnification in V1. In the portion of V1 representing the peripheral visual field, a small amount of tissue responds to a large region in the visual field, whereas in the part of V1 that represents the central visual field, the same amount of tissue responds to only a very small part of the visual field (Figure 4C). Therefore, even though for a given amount of charge the phosphene areas in the visual field spanned a range of about 1,000:1 across sites, the area of activated cortex was tightly clustered. Notably, as the charge increased, the area of activated cortex spread well beyond the size of the electrode (Figure 4B, data points above the dotted lines). The implication is that electrical stimulation cannot be assumed to interact with only cortical regions directly below the stimulated electrode. Rather, with stimulation parameters within the range used for standard clinical testing, we estimate the spatial spread to include an area up to 1 cm^2. The functions fit to phosphene size were power laws, with the exponents less than 1 (Table S4, column 2), indicating that the effect of increasing electrical charge declined with higher stimulation levels, suggesting that the spatial spread saturates with high charge.

Effect of Stimulation Parameters on Subjective Ratings

In addition to obtaining phosphene outlines, for 3 sites we also asked subjects to provide a numerical rating of the intensity of the phosphene. Some of the subjects also offered additional, spontaneous descriptions of phosphene properties (e.g., color, motion), but only the size, location, and intensity of their perceptual change were consistently recorded and thus quantifiable.

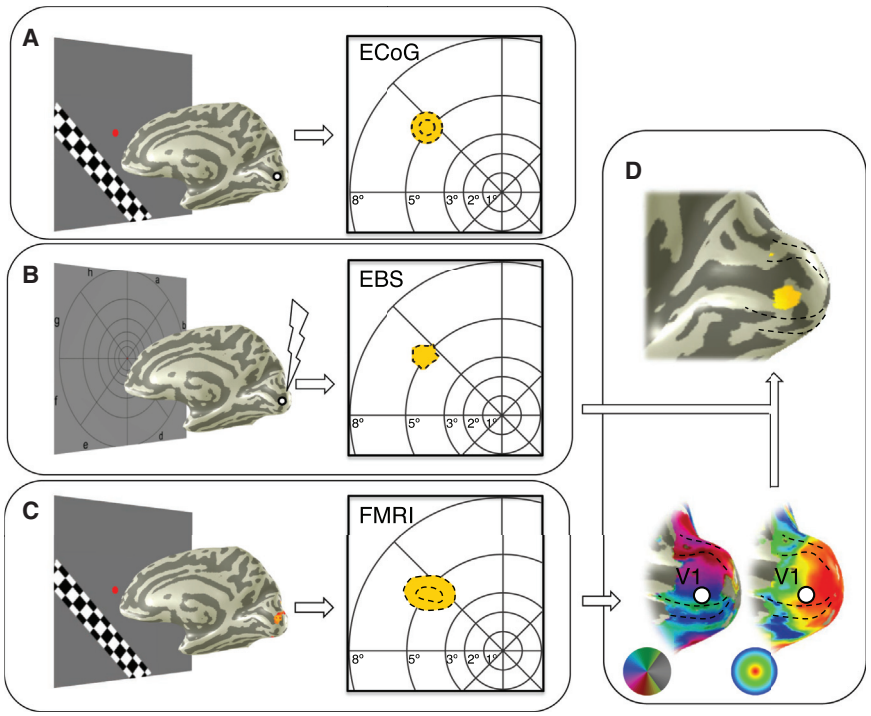

Figure 3. Spatial Selectivity in Human Visual Cortex across 3 Measurement Modalities

(A) A pRF (yellow circle) was computed for the broadband ECoG signal in response to visual stimulation (site 3). Dotted lines show the 1-, and 2-SD lines of the pRF for the electrode indicated on the cortical mesh, as in Figure 2A.

(B) The subject drew the outline of a phosphene during an EBS trial (black dotted line).

(C) The combined fMRI pRFs for voxels near the electrode shown in (A) and (B). Dotted lines as in (A).

(D) The phosphene in (B) was projected onto the cortical surface using the retinotopic map of visual cortex, derived from fMRI.

Like cortical surface area, subjective ratings increased with charge deposited at each site tested but did not depend systematically on the eccentricity of the pRF (Figure 4D). The ratings were most reliable for very low or very high charge, with ratings of 1 or 2 for all trials with charge below 10 μC, and 9 or 10 for all trials with charge above 100 μC. For intermediate charge—between 10 and 100 μC—ratings ranged from 1 to 9. This pattern suggests that perceived intensity, like phosphene size, increased rapidly over intermediate charges and slowly at higher charges. The power law exponent fitted to the ratings ranged from 0.17 and 0.44 (Table S4), indicating that the effect of increasing stimulation decreased at higher stimulation levels.

Next, we separated the charge deposited per site into two complementary components, the amount of charge per phase and the frequency of stimulation. Both parameters influenced the size of the phosphene projected to the cortex: if either the frequency was low (below ~15 Hz) or the charge per phase was low (below ~0.7 μC), the area of responsive tissue on the cortex area was small (Figure 4E, left). In contrast, the subjective rating of intensity only depended systematically on the frequency of stimulation and not on the charge per phase (Figure 4E, right). The difference in these patterns illustrates the value of obtaining multiple quantitative behavioral measures. (See Figure S4 for multiple regression fits.)

DISCUSSION

Our findings are based on a model-based approach to integrate EBS with retinotopic maps, and as such they provide, to our knowledge, the first quantification of the spatial extent of brain tissue affected by EBS in human cerebral cortex. Our results complement estimates made in macaque V1 for stimulation with microelectrodes, using very different stimulation parameters (Tehovnik and Slocum, 2007). Further, the results demonstrate a close quantitative match between visual perception evoked by EBS and neurophysiological responses measured from the human brain. This fact does not bear on the question of whether V1 activity, on its own, is critical for visual awareness (Crick and Koch, 1995), as EBS-induced electrical discharges in V1 propagate to other areas of the brain, enabling the subject to make overt judgments about their experience.

In our data, the broadband ECoG response was the neurophysiological measure that best matched subjective experience, as indexed by the overlap between pRFs and phosphene. These results raise the question of why the pRFs measured by two components of the ECoG time series differ. We consider several possible answers.

First, it might be the case that the two types of pRFs are in fact similar but that the evoked potentials have lower signal-to-noise ratio, leading to a poorer estimation of the pRF for the stimulus-locked signal. This explanation is unlikely, since the evoked signal is large and the variance explained by the two pRF models was nearly identical. Second, the sizes of the neural receptive fields giving rise to the two types of pRFs might differ. This is plausible as different cell types and lamina within the same cortical site can vary substantially in the spatial extent of their responses, as suggested by the large spread of activity in superficial layers measured with voltage-sensitive dye (Palmer et al., 2012). However, this explanation would lead to differences in pRF *size*, whereas we also observe differences in pRF *location*. Hence, this is unlikely to be the complete explanation. A third possibility arises from the fact that the spatial sensitivity of the field potential is highly dependent on the structure of the neural activity, with coherent signals having a significantly longer reach than incoherent signals (Lindén et al., 2011). The implication is that the broadband signal, assuming it has incoherent sources, is dominated by sources close to the electrode (Liu and Newsome, 2006) and is therefore likely a good match to the neurons

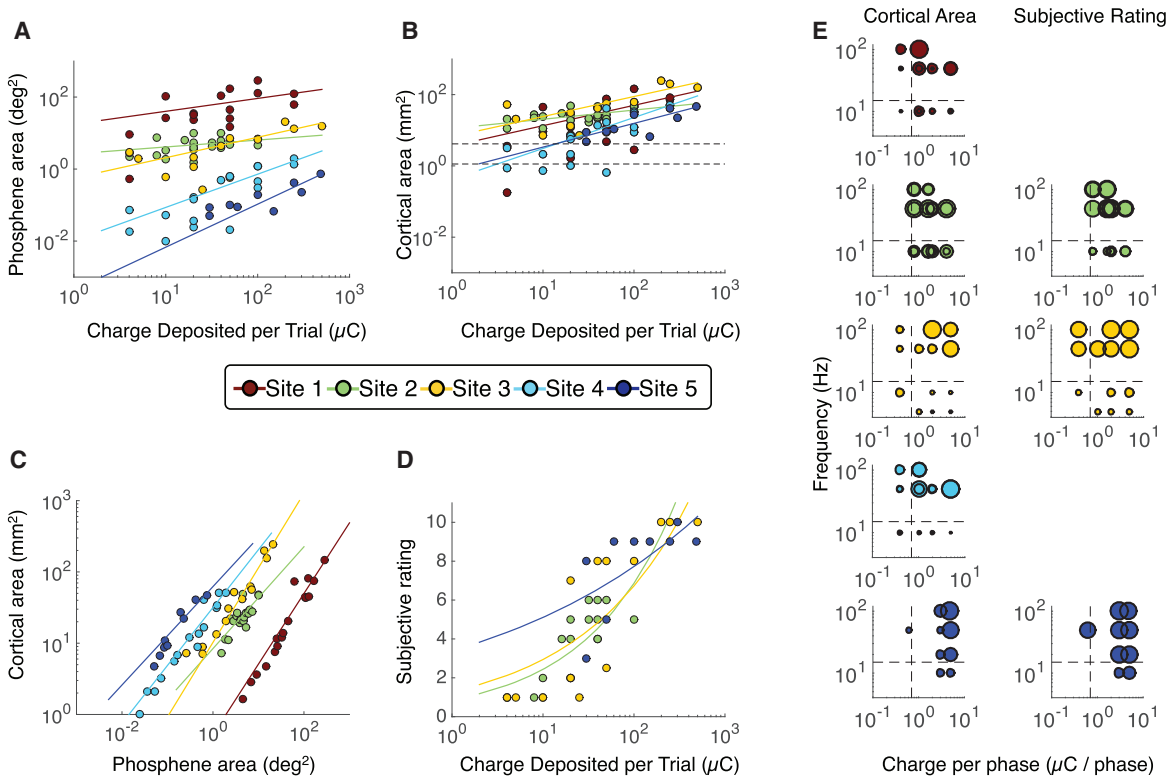

Figure 4. Relationship between Perception and EBS Parameters

(A–D) For all panels, each dot indicates one EBS trial and each color indicates one cortical site. Sites 1 to 5 are numbered by decreasing eccentricity of the site's pRF: site 1 is most peripheral and site 5 is most foveal. For panels (A)–(D), colored lines are the best fitting power functions of the form $y = b*x^m$, fit separately for each site. For parameters and details of fits, see Table S3. Greater charge deposited per EBS trial resulted in (A) larger phosphenes, (B) a larger area of activated cortex (inferred by projecting the phosphenes onto each subject's V1 surface), and (D) a higher subjective intensity rating. The fitted power law exponents are less than 1, indicating that the stimulation effect saturates at high charge. In panel (B), dashed lines indicate the electrode's exposed surface area (upper line for sites 1, 3, 4, and 5; lower line for site 2; see Table S2). Panel (C) shows the relationship between phosphene area in the visual field (x axis) and cortical area (phosphene projected to V1).

(E) The bubble plots separate the charge delivered per trial into charge per phase (x axis) and frequency (y axis). Each bubble indicates one trial, and bubble size reflects either cortical area (left column) or subjective rating (right column). The largest bubble in each plot is scaled to the maximum measurement for that plot (panel B for cortical area and panel D for subjective rating). Dashed lines indicate the stimulation levels that approximately divide the cortical area into large and small values. For a linear model fit to the data in panel (E), see Figure S4 and Table S4.

influenced by EBS. In contrast, the stimulus-locked potential is likely influenced by neurons located at a greater distance. The effect of distance on the pRF will depend on an interaction of the local cortical geometry and the retinotopic map. Finally, we note that cortical generators of the evoked potential (stimulus-locked signal) are not yet fully understood. In cat V1, the evoked potential carries non-retinotopic stimulus information as well as retinotopic (Kitano et al., 1994; Mitzdorf, 1987), which may influence estimates of the receptive field. The broadband signal has been shown to be correlated with both the local BOLD signal and multiunit spiking activity, and likely better reflects the neural activity directly beneath the electrode (Winawer et al., 2013 and references within).

We quantified the effect of EBS on subjective experience with phosphene outlines and numerical ratings. As with all subjective measures, it is important to consider the accuracy with which subjects report their experience. We used an outline task to measure perception with reference to the spatial coordinates of the outline in the tradition of input-referred measures in sensory neuroscience (Wandell, 1995). The outlines on control trials were accurate (matching the visual stimulus) and reliable across repeated trials, providing confidence in the reliability of subjects outlining the phosphene areas. The method was also validated by the high degree of overlap between the EBS outlines and the pRFs from the corresponding electrodes, which do not depend on subjective reports. Rating the intensity of the phosphenes is a less well-defined task and is not measured in physical units. This type of task is in the psychophysical tradition of magnitude estimation (Stevens, 1957). The dependency of ratings on EBS parameters was not identical to the dependency of phosphene area on the EBS parameters, suggesting that the two metrics provide complementary information. As in previous studies of magnitude estimation, the ratings approximately followed a power law. This, and the lack of false positives in sham trials, indicates a degree of validation for this metric.

While our findings have practical implications for the field of neuromodulation, and help us understand better the human EBS literature, several questions remain to be answered: for instance, is the charge spread independent of the cytoarchitecture of the cortical tissue being stimulated; how does the duration of the phosphene depend on the duration of stimulation; and how do the spatial extent and selectivity of the circuits engaged by intracranial EBS compare to stimulation with extracranial techniques used for clinical treatments? These and many more questions were beyond the scope of the present study and will be explored in future studies.

EXPERIMENTAL PROCEDURES

Participants

Four adult patients with focal epilepsy were implanted with intracranial electrodes unilaterally for clinical reasons to localize the source of seizures (age 24 to 40; Table S1). Patients signed informed consent for participation in our study, which was approved by the Stanford University Institutional Review Board.

Electrode Localization

Electrodes were implanted as either strips or grids (AdTech Medical Instrument). Five electrodes were used for analysis from the four patients, all recording from V1 (Table S3). Each electrode was a platinum plate, either 2.3 mm or 1.15 mm in diameter (exposed recording area) with center-to-center spacing of 4–10 mm between adjacent electrodes on the grid or strip. The electrode positions were identified on post-operative computed tomography (CT) images. The CT images were aligned with the preoperative anatomical MRIs using a method described by Hermes et al. (2010).

Anatomical and Functional MRI

MRI sessions were conducted to localize visual field maps and electrode positions. The MRI session took place prior to electrode implantation. In two subjects, we acquired both functional and anatomical MRI (S1 and S3). For S2 and S4, we acquired only anatomical MRI and derived retinotopic maps from the subject's individual anatomy using a retinotopic template (Benson et al., 2014). To verify that each of the electrodes under study was located in V1, two methods were used. First, a V1–V3 template was applied to the T1-weighted whole brain anatomy, and second, a V1 probabilistic atlas was derived from the same T1-weighted anatomy using Freesurfer (Figures 1A and 1B).

Electrophysiological Recording and Artifact Rejection

We recorded signals with a 128-channel recording system made by Tucker Davis Technologies (http://www.tdt.com/). Offline, data were re-referenced to the common average, excluding channels with large artifacts or epileptic activity, as determined by the patient's neurologist (author J.P.).

Visual Mapping Stimuli

Methods for ECoG and fMRI visual field mapping experiments were reported previously in detail (Winawer et al., 2013). A summary of the methods as well as differences from the previous work are described in the Supplemental Experimental Procedures.

PRF Model Fitting

The pRF models were computed as described previously, using a "Compressive Spatial Summation" variant of the linear pRF model (Kay et al., 2013) for the broadband time series and a linear model for the stimulus-locked time series (Eq S1). Formulae and fitting procedures are described in the Supplemental Experimental Procedures.

Broadband and Stimulus-Locked ECoG Responses

The time series of the broadband and stimulus-locked responses to bar stimuli were constructed by short-time Fourier analysis, as previously (Winawer et al., 2013), with one difference. The stimulus-locked time series was defined by the amplitude at 30 Hz, twice the frequency of stimulus contrast reversals, rather than at the frequency of stimulus contrast reversals, as there was a higher signal to noise ratio at this harmonic. Details are included in the Supplemental Experimental Procedures.

Electrical Brain Stimulation

Electrical biphasic, rectangular pulses were delivered at different frequency, pulse width, amplitude, and durations (Table S2). These pulses were current regulated and charge balanced (i.e., no charge accumulation with toxic effect on the tissue). For each site, one electrode was in V1 and the other was in a non-visually responsive region, remote from V1. Occasional sham trials were intermixed with stimulation trials. The subjects were not informed which trials were sham and which contained stimulation. EBS trials took place 1–2 days after ECoG visual mapping experiments (see Table S2 for more details).

Phosphene Recordings

During the EBS sessions, subjects viewed the same laptop used for the ECoG visual mapping experiments, viewed from the same distance. Subjects were instructed to fixate the center of a polar grid prior to EBS (Figure 3B), and to draw the outline of their visual percept on the screen using the laptop touchpad immediately following stimulation. The polar grid provided a spatial reference so that subjects could accurately encode and reproduce the location of the phosphene. Offline, the phosphene outlines were loaded into MATLAB and digitized (Figure S3). Phosphene-pRF overlap was summarized by the Dice Coefficient (Eq S2) and bootstrapped for statistics (Eq S3).

Subjective Ratings

Subjective ratings of phosphene intensity were obtained immediately after drawing the phosphene outline for sites 2, 3, and 5. For site 3 and 5 (S3), the subject was instructed to indicate on a scale from 0–10 how much motion, color, and brightness was in each phosphene. It appeared that the subject did not use the ratings independently, as the three ratings were almost always the same for a given phosphene. Hence, we collapsed the three ratings per trial into one (using the median if the three were not identical). For S2, whose experiment took place later, we asked for only a single rating of 0–10 to indicate the intensity of the percept.

Computation of Phosphene Cortical Area

Phosphenes were projected to the surface of V1 based on the subject's retinotopic map in order to infer the area of activated cortex resulting from EBS. The projection was defined as the set of voxels in V1 whose retinotopic coordinates (x, y) were within the polygon defined by the digitized phosphene. These voxels formed a region of interest, and the surface area of this region of interest was computed on the 3D cortical manifold using methods described previously (Dougherty et al., 2003). The MATLAB function used for this computation is "roiSurfaceArea," part of the freely available in-house vistasoft software (https://github.com/vistalab/vistasoft). The cortical surface area was also estimated using a standard formula that did not depend on each subject's maps (see Supplemental Experimental Procedures).

Data Availability

The software and data used for analyses is available via the Open Science Framework (https://osf.io/pz42u/; DOI: http://dx.doi.org/10.17605/OSF.IO/PZ42U).

SUPPLEMENTAL INFORMATION

Supplemental Information includes Supplemental Experimental Procedures, four figures, and four tables and can be found with this article online at http://dx.doi.org/10.1016/j.neuron.2016.11.008.

AUTHOR CONTRIBUTIONS

J.W. and J.P. designed and executed the studies. J.P. conducted EBS experiments. J.W. analyzed data. J.W. and J.P. wrote the manuscript.

ACKNOWLEDGMENTS

We thank Noah Benson for expert assistance in deriving retinotopic templates for visual cortex. The research was supported by U.S. National Eye Institute (EY022116) to J.W., and U.S. National Institute of Neurological Disorders and Stroke (R01NS078396), U.S. National Institute of Mental Health (1R01MH109954-01), and U.S. National Science Foundation (BCS1358907) to J.P.

Received: October 1, 2016
Revised: October 28, 2016
Accepted: November 1, 2016
Published: December 8, 2016

REFERENCES

Adrian, E.D., and Matthews, B.H.C. (1934). The Berger rhythm: Potential changes from the occipital lobes in man. Brain *57*, 355–385.

Bartholow, R. (1874). Experimental Investigations into the Functions of the Human Brain. Am. J. Med. Sci. *66*, 305–313.

Benson, N.C., Butt, O.H., Brainard, D.H., and Aguirre, G.K. (2014). Correction of distortion in flattened representations of the cortical surface allows prediction of V1-V3 functional organization from anatomy. PLoS Comput. Biol. *10*, e1003538.

Borchers, S., Himmelbach, M., Logothetis, N., and Karnath, H.O. (2011). Direct electrical stimulation of human cortex - the gold standard for mapping brain functions? Nat. Rev. Neurosci. *13*, 63–70.

Brindley, G.S., and Lewin, W.S. (1968). The sensations produced by electrical stimulation of the visual cortex. J. Physiol. *196*, 479–493.

Buzsáki, G., Anastassiou, C.A., and Koch, C. (2012). The origin of extracellular fields and currents–EEG, ECoG, LFP and spikes. Nat. Rev. Neurosci. *13*, 407–420.

Canolty, R.T., Edwards, E., Dalal, S.S., Soltani, M., Nagarajan, S.S., Kirsch, H.E., Berger, M.S., Barbaro, N.M., and Knight, R.T. (2006). High gamma power is phase-locked to theta oscillations in human neocortex. Science *313*, 1626–1628.

Cohen, M.R., and Newsome, W.T. (2004). What electrical microstimulation has revealed about the neural basis of cognition. Curr. Opin. Neurobiol. *14*, 169–177.

Crick, F., and Koch, C. (1995). Are we aware of neural activity in primary visual cortex? Nature *375*, 121–123.

Crone, N.E., Miglioretti, D.L., Gordon, B., and Lesser, R.P. (1998). Functional mapping of human sensorimotor cortex with electrocorticographic spectral analysis. II. Event-related synchronization in the gamma band. Brain *121*, 2301–2315.

Dobelle, W.H., and Mladejovsky, M.G. (1974). Phosphenes produced by electrical stimulation of human occipital cortex, and their application to the development of a prosthesis for the blind. J. Physiol. *243*, 553–576.

Dougherty, R.F., Koch, V.M., Brewer, A.A., Fischer, B., Modersitzki, J., and Wandell, B.A. (2003). Visual field representations and locations of visual areas V1/2/3 in human visual cortex. J. Vis. *3*, 586–598.

Dumoulin, S.O., and Wandell, B.A. (2008). Population receptive field estimates in human visual cortex. Neuroimage *39*, 647–660.

Foerster, O. (1929). Beitriige zur Pathophysiologie der Sehbahn und der Sehsphare. J. Psychol. Neurol. *39*, 463–485.

Hermes, D., Miller, K.J., Noordmans, H.J., Vansteensel, M.J., and Ramsey, N.F. (2010). Automated electrocorticographic electrode localization on individually rendered brain surfaces. J. Neurosci. Methods *185*, 293–298.

Hinds, O.P., Rajendran, N., Polimeni, J.R., Augustinack, J.C., Wiggins, G., Wald, L.L., Diana Rosas, H., Potthast, A., Schwartz, E.L., and Fischl, B. (2008). Accurate prediction of V1 location from cortical folds in a surface coordinate system. Neuroimage *39*, 1585–1599.

Histed, M.H., Bonin, V., and Reid, R.C. (2009). Direct activation of sparse, distributed populations of cortical neurons by electrical microstimulation. Neuron *63*, 508–522.

Kay, K.N., Winawer, J., Mezer, A., and Wandell, B.A. (2013). Compressive spatial summation in human visual cortex. J. Neurophysiol. *110*, 481–494.

Kitano, M., Niiyama, K., Kasamatsu, T., Sutter, E.E., and Norcia, A.M. (1994). Retinotopic and nonretinotopic field potentials in cat visual cortex. Vis. Neurosci. *11*, 953–977.

Lindén, H., Tetzlaff, T., Potjans, T.C., Pettersen, K.H., Grün, S., Diesmann, M., and Einevoll, G.T. (2011). Modeling the spatial reach of the LFP. Neuron *72*, 859–872.

Liu, J., and Newsome, W.T. (2006). Local field potential in cortical area MT: stimulus tuning and behavioral correlations. J. Neurosci. *26*, 7779–7790.

Miller, K.J., Sorensen, L.B., Ojemann, J.G., and den Nijs, M. (2009). Power-law scaling in the brain surface electric potential. PLoS Comput. Biol. *5*, e1000609.

Miller, K.J., Honey, C.J., Hermes, D., Rao, R.P., denNijs, M., and Ojemann, J.G. (2014). Broadband changes in the cortical surface potential track activation of functionally diverse neuronal populations. Neuroimage *85*, 711–720.

Milstein, J., Mormann, F., Fried, I., and Koch, C. (2009). Neuronal shot noise and Brownian 1/f2 behavior in the local field potential. PLoS ONE *4*, e4338.

Mitzdorf, U. (1987). Properties of the evoked potential generators: current source-density analysis of visually evoked potentials in the cat cortex. Int. J. Neurosci. *33*, 33–59.

Norcia, A.M., Appelbaum, L.G., Ales, J.M., Cottereau, B.R., and Rossion, B. (2015). The steady-state visual evoked potential in vision research: A review. J. Vis. *15*, 4.

Ojemann, G., Ojemann, J., Lettich, E., and Berger, M. (1989). Cortical language localization in left, dominant hemisphere. An electrical stimulation mapping investigation in 117 patients. J. Neurosurg. *71*, 316–326.

Palmer, C.R., Chen, Y., and Seidemann, E. (2012). Uniform spatial spread of population activity in primate parafoveal V1. J. Neurophysiol. *107*, 1857–1867.

Penfield, W., and Perot, P. (1963). The brain's record of auditory and visual experience. a final summary and discussion. Brain *86*, 595–696.

Salzman, C.D., Britten, K.H., and Newsome, W.T. (1990). Cortical microstimulation influences perceptual judgements of motion direction. Nature *346*, 174–177.

Stevens, S.S. (1957). On the psychophysical law. Psychol. Rev. *64*, 153–181.

Tehovnik, E.J., and Slocum, W.M. (2007). Phosphene induction by microstimulation of macaque V1. Brain Res. Brain Res. Rev. *53*, 337–343.

Wandell, B.A. (1995). Foundations of Vision (Sinauer Associates).

Winawer, J., Kay, K.N., Foster, B.L., Rauschecker, A.M., Parvizi, J., and Wandell, B.A. (2013). Asynchronous broadband signals are the principal source of the BOLD response in human visual cortex. Curr. Biol. *23*, 1145–1153.

Yoshor, D., Bosking, W.H., Ghose, G.M., and Maunsell, J.H. (2007). Receptive fields in human visual cortex mapped with surface electrodes. Cereb. Cortex *17*, 2293–2302.

Neuron, Volume *92*

Supplemental Information

Linking Electrical Stimulation of Human Primary Visual Cortex, Size of Affected Cortical Area, Neuronal Responses, and Subjective Experience

Jonathan Winawer and Josef Parvizi

Figure S1. Related to Figure 1.

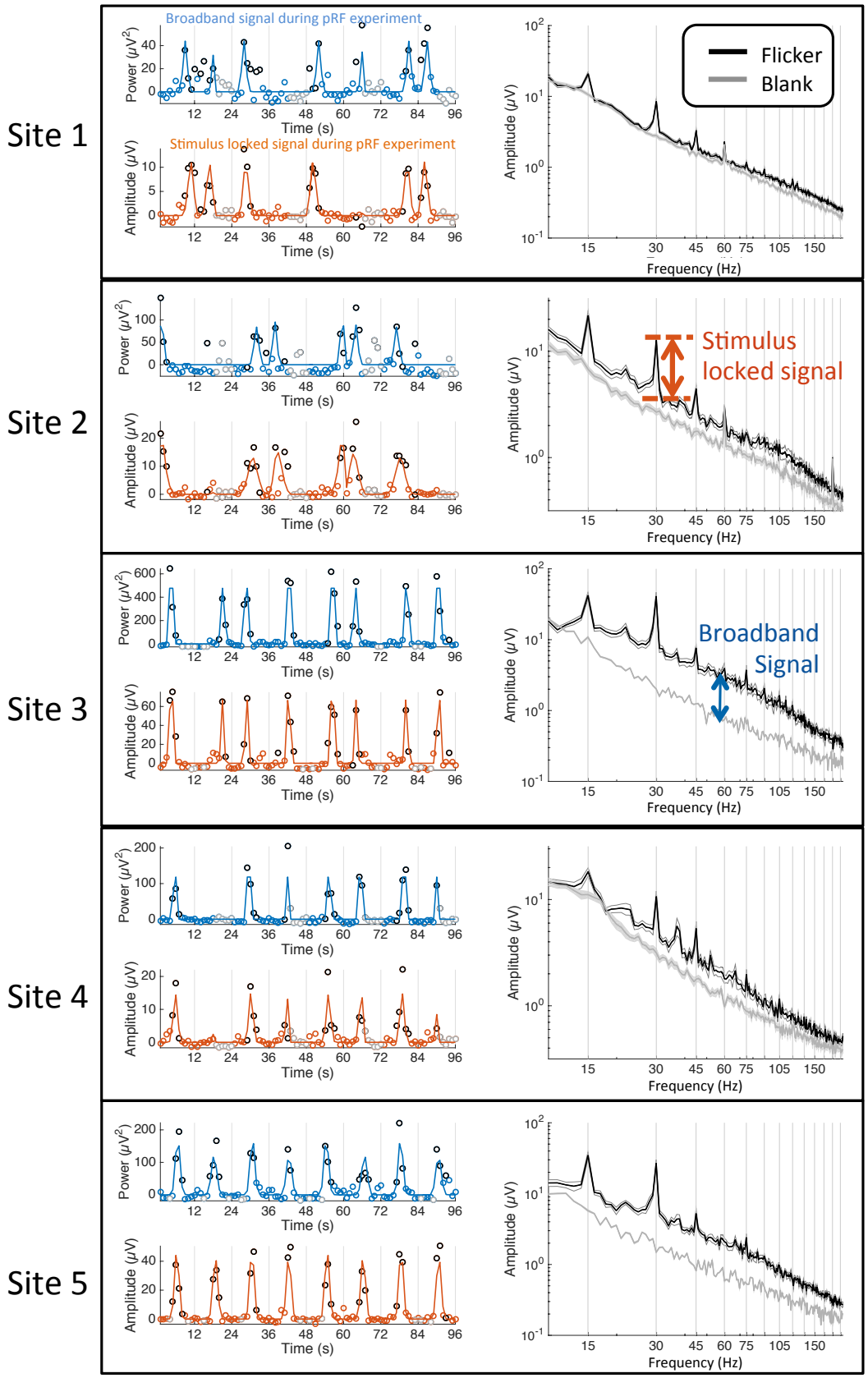

Figure S1. Related to Figure 1. Separation of ECoG signal into stimulus-locked and broadband components. Broadband and stimulus locked responses for each of 5 sites. See Figure 1C,D for details. The data for site 2 are also plotted 1C,D.

Figure S2. Related to Figure 2.

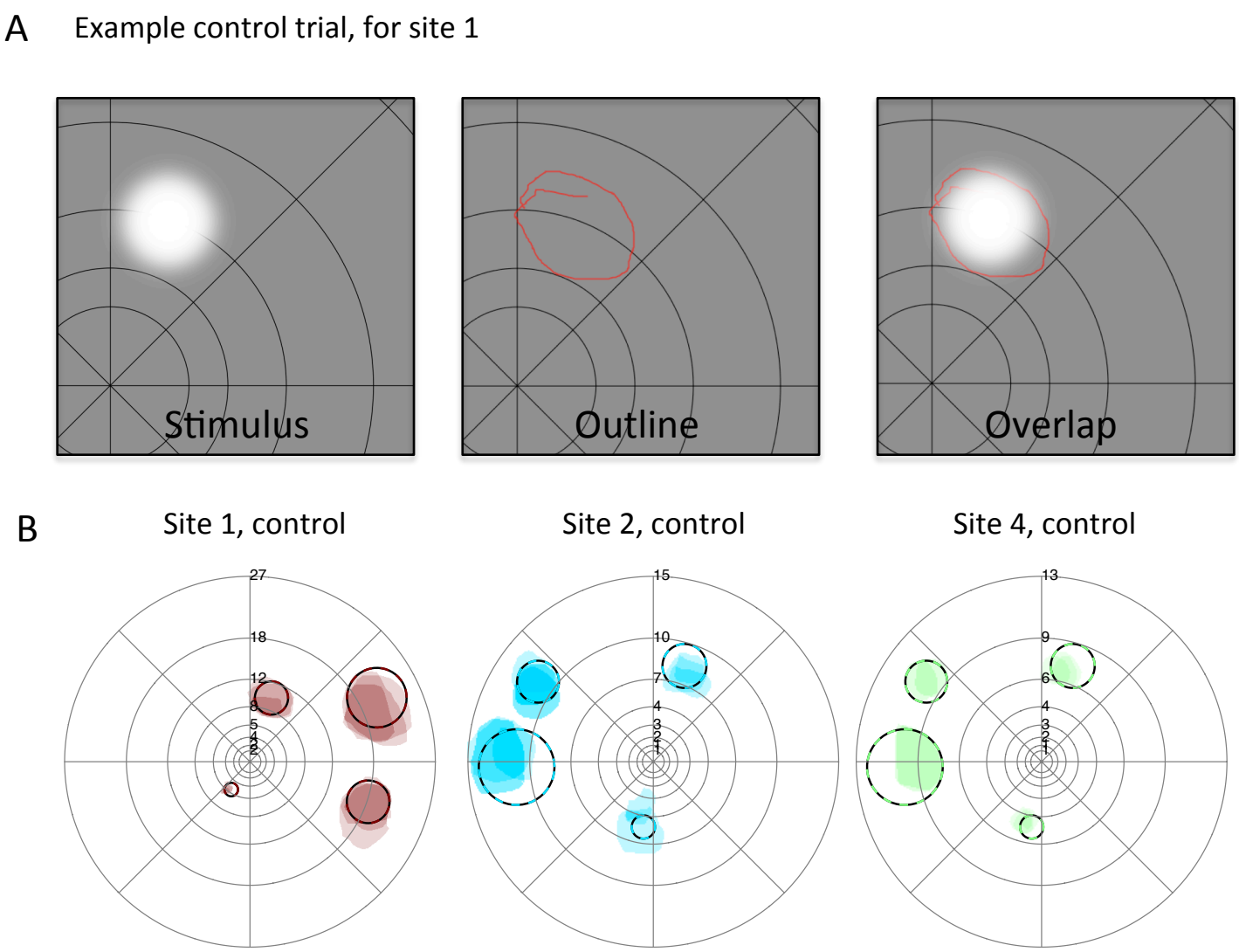

Figure S2. Related to Figure 2. Drawing reliability on control trials. To assess whether subjects could reliably outline visual sensations, control trials were conducted in which subjects marked the locations of briefly viewed stimuli. (A) The stimuli were white circles with a smoothed edge on a gray background with a black, polar grid (left). The visual stimuli were presented for one second while the subject fixated the center of the grid. Immediately after the stimulus disappeared, the subject outlined the region where it was presented (middle). The overlap for this trial (control for site 1) shows excellent agreement between stimulus and outline (right). (B) Stimuli were presented in 4 locations 3 times each in random order for each subject. Stimuli close to fixation were smaller than those in the periphery. Each panel shows all 12 control trials from one subject. The locations of the stimuli are indicated as dashed outlines. The subjects' drawings are shown as partially transparent shaded regions for consistency with Figures 3 and 4. The three subjects tested in the control trials are the subjects with electrodes at sites 1, 2, and 4 for ECoG and EBS trials. (The subject with EBS/ECoG sites 3 and 5 was not tested in this control procedure.) Overall there is good agreement between the stimulus locations (outlines) and the subject drawings (shaded regions), indicating that subjects understood and could do the task.

Figure S3. Related to Figure 2.

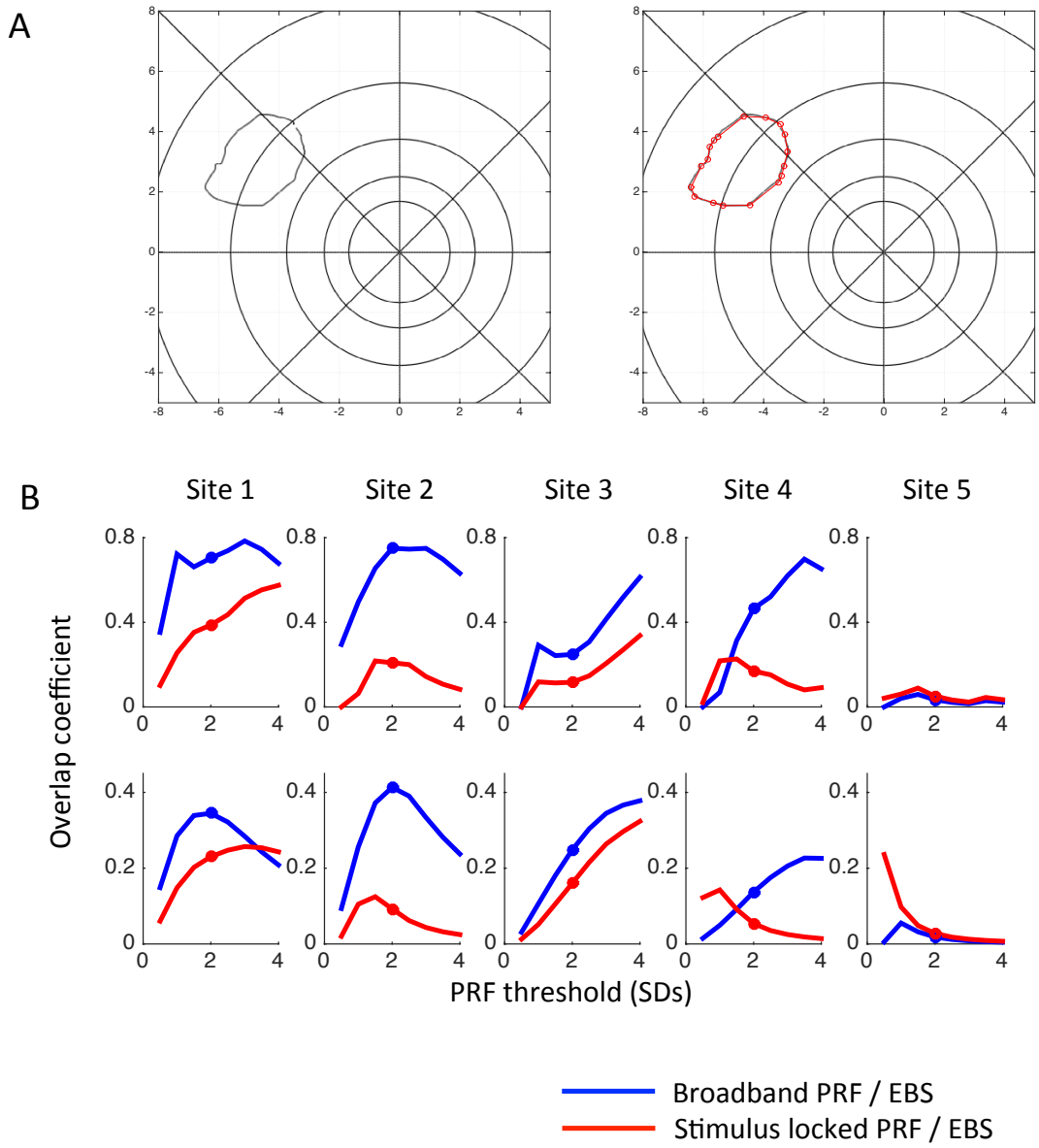

Figure S3. Related to Figure 2. Overlap between phosphenes and pRFs. (A) An example screen capture of a phosphene drawn by S3 is shown on the left. The polar grid was seen during the EBS trial to facilitate accurate encoding and reproduction of the phosphene. On the right is the manual digitization of the phosphene, indicated in red. (B) For each of 5 sites, two pRFs were obtained, one from the ECoG broadband signal and one from the ECoG stimulus locked signal. For each site there were multiple EBS trials, with 9 to 21 phosphenes per site. Overlap between the phosphenes and the pRFs was summarized by the Sørensen-Dice coefficient (2 times the area of overlap divided by the sum area of the two areas). The upper plots show the overlap computed between the pRF at each site with the average phosphene from that site, and the lower plots show the average of the overlap between the pRF from a site and each of the separate phosphenes from that site. For the upper plot, the average of the phosphenes was defined by first averaging the binarized phosphene images (1s inside the outline, 0s outside), and then thresholding the resultant image. The threshold value was expressed in standard deviations: A threshold of *n* STDs was defined as a Gaussian with height 1 evaluated at radius *n STDs:* $e^{-\frac{n^2}{2}}$. The pRFs were also thresholded at *n STDs*. The x-axis indicates different thresholds in units of STDs. The y-axis is the overlap coefficient. A threshold of 2, indicated by a circle on each plot, was used to summarize the data in the main text and in Supplementary table 1. The lower panels plot the overlap by computing the Sørensen dice coefficient for the thresholded pRF and each phosphene separately, yielding 9 to 21 overlaps for each site. The mean of these overlaps is plotted. For sites 1-4, the overlap is higher for the broadband pRFs than the stimulus locked pRFs at nearly any threshold evaluated by either method (overlap between pRF and mean of phosphenes, or mean overlap between pRFs and phosphenes). For site 5, the overlap was higher for the stimulus locked pRF, although the overlap coefficient was low for both kinds of pRFs.

Figure S4. Related to Figure 4.

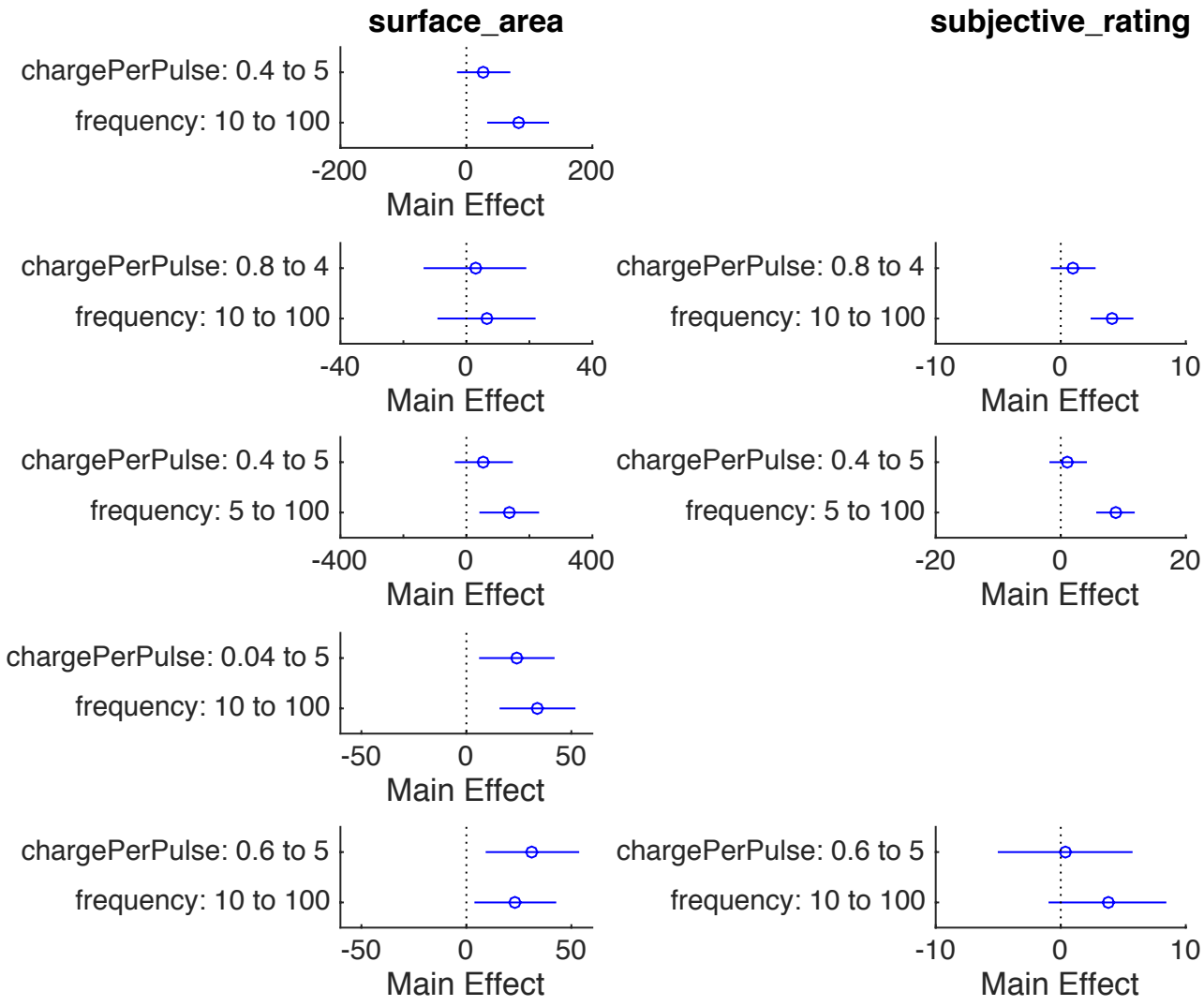

Figure S4. Related to Figure 4. Model fits for Figure 4E. Plots show the parameter fits for a linear model in which either phosphene surface area (left) or subjective rating (right) were predicted by the charge per pulse and the frequency of stimulation, corresponding to Figure 4E. Rows 1-5 correspond to sites 1-5. Circles indicate the mean and the line indicates the 95% parameter fit. For example, for site 5, varying the frequency from 10 to 100 Hz caused an increase in surface area of about 25±20 mm^2, and varying the charge per pulse from 0.6 µC to 5 µC caused an increase in surface area of about 35±25 mm^2. In 4 of 5 sites, the effect of frequency on phosphene surface area was greater than 0 (95% CI), and in 2 of 5 sites, the effect of charge per pulse on surface area was greater than 0. For subjective rating, frequency had a clear effect in 2 of 3 sites, and a marginal effect in the third. Charge per pulse did not have a significant effect on the subjective rating in any of the three sites.

Table S1. Related to Figure 1.

Site #	Subject number	Hemi	Gender	Age	Electrode Diameter (mm)	Diameter of exposed electrode (mm)	Spacing between electrodes (mm)	Recording frequency (Hz)	Seizure Zone (Pathology)
1	1	L	M	24	4	2.3	5	1525.88	Posterior collateral sulcus (cortical dysplasia)
2	2	R	M	36	2	1.2	4	1000.00	Lateral occipital (not resected, pathology unavailable)
3	3	R	M	40	4	2.3	5	3051.76	Medial fusiform gyrus (cortical dysplasia)
4	4	R	F	36	4	2.3	5	1525.88	Medial temporal lobe (gliosis)
5	3	R	M	40	4	2.3	5	3051.76	Medial fusiform gyrus (cortical dysplasia)

Table S1. Participant details. The study comprised of 5 V1 sites (column 1) in 4 subjects (column 2). Participant details in columns 3-5 indicate the hemisphere of the implantation, the gender, and the age at the time of the experiment. The exposed electrode diameter (column 7) is defined in terms of the region of exposed platinum. Spacing (column 8) is the center-to-center spacing on the strip or grid. The recording frequency (column 9) was several times above the high end of the band pass filter.. The seizure zone in all subjects (column 10) was remote from primary visual cortex.

Table S2. Related to Figure 2.

Site	Trial #	Current (mA)	Frequency (Hz)	Pulse Width (μS)	Duration (S)	Charge per Pulse (μC)	Charge per Trial (μC)	Rating (1-10)	Phosphene Area (deg^2)	Cortical Area, Individual V1 (mm^2)	Cortical Area, Formula (mm^2)
1	1	5	50	200	1	1	50	–	45.0	22.5	20.4
1	2	5	10	1000	1	5	50	–	15.0	4.1	4.7
1	3	5	50	1000	1	5	250	–	61.6	74.4	74.3
1	4	2	10	1000	1	2	20	–	35.3	14.5	14.1
1	5	2	50	1000	1	2	100	–	6.9	0.0	2.9
1	6	2	10	200	1	0.4	4	–	0.5	0.0	0.2
1	7	5	10	200	1	1	10	–	26.1	9.3	9.1
1	8	2	50	200	1	0.4	20	–	23.0	7.8	7.7
1	9	2	10	1000	1	2	20	–	32.3	11.1	12.2
1	10	2	50	200	1	0.4	20	–	4.6	0.0	1.7
1	11	2	50	1000	1	2	100	–	127.9	43.2	45.3
1	12	5	50	1000	1	5	250	–	124.1	74.9	82.0
1	13	5	10	1000	1	5	50	–	25.0	13.5	11.7
1	14	2	10	200	1	0.4	4	–	9.2	2.9	3.6
1	15	5	10	200	1	1	10	–	106.1	42.1	44.7
1	16	5	50	200	1	1	50	–	167.4	69.1	76.2
1	17	2	100	200	1	0.4	40	–	108.1	40.1	43.9
1	18	5	100	200	1	1	100	–	286.3	153.8	146.7
2	1	2	50	400	0.5	0.8	20	–	10.0	48.0	36.3
2	2	4	50	1000	0.5	4	100	5	4.6	55.0	37.0
2	3	4	10	1000	0.5	4	20	2	1.6	4.5	5.5
2	4	2	50	1000	0.5	2	50	6	5.9	28.6	20.4
2	5	4	10	400	0.5	1.6	8	–	7.3	27.4	20.8
2	6	Sham						–	–	–	–
2	7	4	50	400	0.5	1.6	40	6	10.0	46.4	35.2
2	8	Sham						–	–	–	–
2	9	4	100	400	0.2	1.6	32	6	5.3	14.1	12.6
2	10	2	10	1000	0.5	2	10	2	1.9	11.1	8.5
2	11	2	10	400	0.5	0.8	4	1	2.2	12.0	8.4
2	12	4	10	1000	0.5	4	20	2	3.4	23.3	20.2
2	13	2	50	400	0.5	0.8	20	5	5.4	27.7	19.9
2	14	2	100	400	0.5	0.8	40	5	4.0	20.1	16.0
2	15	Sham						–	–	–	–
2	16	2	10	1000	0.5	2	10	1	3.3	23.7	17.9
2	17	4	10	400	0.5	1.6	8	1	2.4	20.0	16.7
2	18	2	10	400	0.5	0.8	4	1	2.8	18.0	15.5
2	19	2	50	1000	0.5	2	50	5	4.7	18.9	15.4
2	20	Sham						–	–	–	–

Site	Trial #	Current (mA)	Frequency (Hz)	Pulse Width (μS)	Duration (S)	Charge per Pulse (μC)	Charge per Trial (μC)	Rating (1-10)	Phosphene Area (deg^2)	Cortical Area, Individual V1 (mm^2)	Cortical Area, Formula (mm^2)
2	21	4	50	400	0.5	1.6	40	4	4.8	22.9	17.5
2	22	2	50	1000	0.2	2	20	4	3.9	19.4	14.5
2	23	2	100	400	0.2	0.8	16	4	6.4	29.5	22.0
2	24	4	50	1000	0.2	4	40	4	6.0	26.2	19.6
2	25	4	100	400	0.2	1.6	32	5	4.2	21.5	15.9
3	1	Sham						–	–	–	–
3	2	5	10	1000	1	5	50	2.5	0.6	11.9	7.1
3	3	5	50	1000	1	5	250	10	13.3	235.3	159.1
3	4	5	5	1000	1	5	25	1	0.3	0.0	5.8
3	5	5	100	1000	1	5	500	10	15.2	200.3	123.9
3	6	5	100	200	1	1	100	7	–	–	–
3	7	Sham						–	–	–	–
3	8	5	50	200	1	1	50	8	7.2	75.0	45.0
3	9	5	10	200	1	1	10	1	–	–	–
3	10	Sham						–	–	–	–
3	11	5	5	200	1	1	5	1	2.0	25.4	16.5
3	12	1	5	200	1	0.2	1	1	–	–	–
3	13	2	100	200	1	0.4	40	8	4.4	58.7	33.3
3	14	2	50	200	1	0.4	20	7	2.2	39.9	24.4
3	15	2	10	200	1	0.4	4	1	2.9	69.9	41.5
3	16	2	10	1000	1	2	20	2	1.2	17.6	10.7
3	17	2	100	1000	1	2	200	10	20.8	294.0	194.5
3	18	Sham						–	–	–	–
3	19	Sham						–	–	–	–
3	20	2	5	1000	1	2	10	1	0.6	8.6	5.7
3	21	2	50	1000	1	2	100	8	6.7	81.1	49.5
4	1	2	50	200	1	0.4	20	–	0.2	13.7	10.5
4	2	2	10	200	1	0.4	4	–	0.1	7.8	5.0
4	3	2	10	200	1	0.4	4	–	0.02	0.0	1.3
4	4	2	50	200	1	0.4	20	–	0.1	10.0	8.7
4	5	2	100	200	1	0.4	40	–	0.5	21.3	21.1
4	6	2	10	1000	1	2	20	–	0.02	0.0	1.6
4	7	2	50	1000	1	2	100	–	0.5	14.8	13.8
4	8	2	10	1000	1	2	20	–	0.04	0.0	3.2
4	*9*	*0.2*	*50*	*200*	*1*	*0.04*	*2*	–	*No phosphene*		
4	10	2	50	1000	1	2	100	–	0.3	20.7	18.7
4	11	5	10	200	1	1	10	–	0.1	5.1	3.2
4	12	5	50	200	1	1	50	–	0.6	27.0	25.9
4	13	5	100	200	1	1	100	–	1.2	42.0	52.7
4	*14*	*5*	*10*	*1000*	*1*	*5*	*50*	–	*No phosphene*		

Site	Trial #	Current (mA)	Frequency (Hz)	Pulse Width (μS)	Duration (S)	Charge per Pulse (μC)	Charge per Trial (μC)	Rating (1-10)	Phosphene Area (deg^2)	Cortical Area, Individual V1 (mm^2)	Cortical Area, Formula (mm^2)
4	15	5	50	1000	1	5	250	–	1.9	79.9	78.5
4	16	5	10	200	1	1	10	–	0.01	0.0	1.1
4	17	5	50	200	1	1	50	–	0.6	45.0	63.2
4	18	5	100	200	1	1	100	–	1.2	46.4	48.3
4	19	5	10	1000	1	5	50	–	0.02	0.0	1.0
4	20	5	50	1000	1	5	250	–	1.4	67.4	78.4
5	*1*	*1*	*50*	*200*	*1*	*0.2*	*10*	–	*No phosphene*		
5	2	3	50	200	1	0.6	30	8	0.1	7.2	5.5
5	3	3	10	200	1	0.6	6	2	Phosphene seen, drawing not obtained		
5	4	3	100	200	1	0.6	60	10	Phosphene seen, drawing not obtained		
5	5	3	20	200	1	0.6	12	2	Phosphene seen, drawing not obtained		
5	6	Sham						–	–	–	–
5	7	Sham						–	–	–	–
5	8	3	20	1000	1	3	60	9	0.1	14.1	12.8
5	9	3	100	1000	1	3	300	10	0.2	37.2	26.1
5	10	Sham						–	–	–	–
5	11	3	10	1000	1	3	30	3	0.1	13.4	10.1
5	12	3	50	1000	1	3	150	9	0.1	11.2	7.8
5	13	5	50	1000	1	5	250	9	0.4	62.0	47.2
5	*14*	*5*	*50*	*1000*	*1*	*5*	*250*	–	*No phosphene*		
5	15	Sham						–	–	–	–
5	16	5	10	1000	1	5	50	5	0.1	16.5	10.9
5	17	5	20	1000	1	5	100	9	0.2	30.3	31.7
5	18	4.84	100	1000	1	4.84	484	9	0.7	74.6	54.4

Table S2. EBS results in all trials. EBS results are listed by site (1-5) and by trial number. For each trial we indicate the current (mA) , frequency (Hz), pulse width (μS) and duration (S). The charge per pulse, in μC, is the product of pulse width in ms and current in mA. Charge deposited per trial in μC is the product of charge per pulse in μC, frequency in Hz, and duration in seconds. The subjective rating on a 1-10 scale was obtained for sites 2, 3, and 5. For sites 2 and 3, the subject separately rated the intensity of color, brightness, and motion, each on a 1-10 scale. But since the three values were almost always the same, we collapsed them into 1 (using the median if the three were not identical). The phosphene area (deg^2) was computed by digitizing the points on the subject's outline and measuring the area within the outline. The cortical area for individual V1 (mm^2) is the projection of the phosphene onto the subject's V1 map. The cortical area by formula was computed by assuming a standard formula for cortical magnification (see Methods). Of the 102 trials, there were 13 sham trials (no stimulation) and there were no false positives. Of the 89 trials with stimulation, there were 4 trials in which no phosphene was reported. There were 3 trials in which phosphenes were reported but no drawing was obtained.

Table S3. Related to Figure 2.

	pRF variance explained		Sørensen–Dice coefficient between ECoG pRF and mean of phosphenes		Mean Sørensen–Dice coefficient between ECoG pRF and individual phosphenes		Bootstraps in which Broadband Sørensen–Dice coefficient is higher than SL coefficient	
Site	**Broadband**	**Stimulus-locked**	**Broadband**	**Stimulus-locked**	**Broadband**	**Stimulus-locked**	**Fraction**	**P-Value**
1	64.0	83.3	0.70	0.39	0.34	0.23	0.0093	0.0186
2	81.8	74.3	0.75	0.21	0.41	0.09	0.0000	0.0000
3	87.9	86.2	0.25	0.12	0.25	0.16	0.0000	0.0000
4	84.9	68.6	0.46	0.17	0.14	0.05	0.0030	0.0060
5	85.0	89.0	0.03	0.05	0.02	0.03	1.0000	0.0000

Table S3. EBS and ECoG overlap. For each of 5 sites, a pRF was measured from the ECoG broadband time series and the ECoG stimulus-locked time series. The table show the variance explained in these time series by the pRF model (columns 2-3). The Sørensen-Dice coefficient was computed in two ways. First, it was computed as the overlap between the thresholded pRF and the thresholded and averaged phosphene for that site (columns 4 and 5). Second, it was computed as the average overlap between the thresholded pRF and each separate phosphene, and then averaged across phosphenes for that site (columns 6 and 7). The first method yields higher overlap values, but it provides only one overlap coefficient per site for broadband and one for the stimulus locked signal. The second method results in multiple overlap coefficients at each site (9-21 phosphenes per site, each compared with the broadband pRF and the stimulus locked pRF). To assess statistical significance of the difference in overlap between the phosphenes and broadband versus stimulus-locked pRFs, the paired overlap coefficients for each site (9-21) were bootstrapped 10,000 times, and the mean of the differences between the pairs was computed 10,000 times. The 8th column shows the fraction of bootstraps for which the overlap between broadband pRF and phosphenes was higher than stimulus-locked pRF and phosphenes. The 9th column converts this fraction into a two-tailed *p-value* by the formula, $1 - 2 \times \mathrm{abs}(0.5 - fraction)$.

Table S4. Related to Figure 4.

Site	**Figure 4a** Phosphene area (deg^2) v charge deposited per trial(μC)	**Figure 4b** Cortical area (mm^2) v charge deposited per trial(μC)	**Figure 4c** Cortical area (mm^2) v Phosphene area (deg^2)	**Figure 4d** Subjective rating v Charge deposited per trial (μC)
1	General model: f(x) = b*x^m Coefficients (with 95% CI): b = 3.609 (-4.598, 11.82) **m = 0.5709 (0.1032, 1.039)** sse: 1.6569e+04 rsquare: 0.3648 dfe: 16 adjrsquare: 0.3251 rmse: 32.1803	General model: f(x) = b*x^m Coefficients (with 95% CI): b = 17.62 (-19.69, 54.94) m = 0.358 (-0.1094, 0.8254) sse: 7.7123e+04 rsquare: 0.1834 dfe: 16 adjrsquare: 0.1323 rmse: 69.4275	General model: f(x) = b*x^m Coefficients (with 95% CI): b = 0.5213 (-0.1538, 1.196) m = 0.9901 (0.7412, 1.239)	General model: f(x) = b*x^m Coefficients (with 95% CI): b = 0.8658 (0.1519, 1.58) **m = 0.4495 (0.2222, 0.6768)** sse: 23.9083 rsquare: 0.6045 dfe: 16 adjrsquare: 0.5797 rmse: 1.2224
2	General model: f(x) = b*x^m Coefficients (with 95% CI): b = 11.24 (1.846, 20.64) **m = 0.2577 (0.01383, 0.5015)** sse: 2.0083e+03 rsquare: 0.2030 dfe: 19 adjrsquare: 0.1610 rmse: 10.2810	General model: f(x) = b*x^m Coefficients (with 95% CI): b = 2.638 (0.2192, 5.058) m = 0.1921 (-0.08092, 0.4652) sse: 94.9695 rsquare: 0.1208 dfe: 19 adjrsquare: 0.0745 rmse: 2.2357	General model: f(x) = b*x^m Coefficients (with 95% CI): b = 8.406 (3.981, 12.83) m = 0.714 (0.4226, 1.005)	
3	General model: f(x) = b*x^m Coefficients (with 95% CI): b = 6.636 (-6.022, 19.29) **m = 0.5624 (0.217, 0.9077)** sse: 2.6131e+04 rsquare: 0.6473 dfe: 11 adjrsquare: 0.6152 rmse: 48.7395	General model: f(x) = b*x^m Coefficients (with 95% CI): b = 0.5586 (-0.3825, 1.5) **m = 0.5678 (0.2632, 0.8724)** sse: 150.6532 rsquare: 0.7090 dfe: 11 adjrsquare: 0.6825 rmse: 3.7008	General model: f(x) = b*x^m Coefficients (with 95% CI): b = 10.26 (2.999, 17.53) m = 1.046 (0.7889, 1.303)	General model: f(x) = b*x^m Coefficients (with 95% CI): b = 1.288 (-0.01894, 2.595) **m = 0.3589 (0.1607, 0.5571)** sse: 62.7857 rsquare: 0.6582 dfe: 11 adjrsquare: 0.6271 rmse: 2.3891
4	General model: f(x) = b*x^m Coefficients (with 95% CI): b = 0.417 (-0.3412, 1.175) **m = 0.8684 (0.5138, 1.223)** sse: 1.6760e+03 rsquare: 0.7082 dfe: 18 adjrsquare: 0.6919 rmse: 9.6493	General model: f(x) = b*x^m Coefficients (with 95% CI): b = 0.01028 (-0.007065, 0.02763) **m = 0.9227 (0.5961, 1.249)** sse: 1.3659 rsquare: 0.7740 dfe: 18 adjrsquare: 0.7614 rmse: 0.2755	General model: f(x) = b*x^m Coefficients (with 95% CI): b = 31.64 (27.34, 35.95) m = 0.8123 (0.5716, 1.053)	
5	General model: f(x) = b*x^m Coefficients (with 95% CI): b = 0.7267 (-1.205, 2.659) **m = 0.6657 (0.1967, 1.135)** sse: 576.8872 rsquare: 0.7000 dfe: 7 adjrsquare: 0.6571 rmse: 9.0781	General model: f(x) = b*x^m Coefficients (with 95% CI): b = 0.0004315 (-0.00124, 0.002103) **m = 1.195 (0.542, 1.848)** sse: 0.0684 rsquare: 0.8373 dfe: 7 adjrsquare: 0.8141 rmse: 0.0989	General model: f(x) = b*x^m Coefficients (with 95% CI): b = 62.28 (47.97, 76.59) m = 0.6905 (0.4908, 0.8901)	General model: f(x) = b*x^m Coefficients (with 95% CI): b = 3.382 (0.02973, 6.735) m = 0.1792 (-0.01639, 0.3749) sse: 24.7070 rsquare: 0.4239 dfe: 7 adjrsquare: 0.3416 rmse: 1.8787

Table S4. Power function model fits for Figure 4A-D. The table shows model fits for each of 5 sites for plots in Figure 4A-D (with only 3 sites for 4d). Data were fit with a power law of the form, *f(x) = b*x^m*. The table shows the estimated coefficients (*b* and *m)* and 95% CI, the sum of squared error (sse), rsquare, degrees of freedom (dfe), adjrsquare, and root mean squared error (rmse). When the lower end of the 95% CI of the *m* parameter is positive, the fit indicates a significantly positive slope (indicated in **bold**). Statistics indicating goodness of fit are omitted from the column for Figure 4C because the data on the y-axis (cortical area) was derived in part from the data on the x-axis, so that the two variables are not independent.

Supplemental Experimental Procedures

Participants

Four adult patients with focal epilepsy were implanted with intracranial electrodes unilaterally for clinical reasons to localize the source of seizures. There were 3 male patients and 1 female (age 24 to 40; Table S1). All subjects had normal or corrected-to-normal vision. Prior to implantation of electrodes, patients performed structural MRI as well as functional MRI, and after surgery, patients were monitored with implanted electrodes during the same visual mapping task (see below). Patients signed informed consent for participation in our study, which was approved by the Stanford University Institutional Review Board. In each patient, V1 and adjacent cortex was outside the seizure onset zone and void of epileptiform activity.

Electrode localization

Electrodes were implanted as either strips or grids (AdTech Medical Instrument Corp, Racine, Wisconsin, USA). Five electrodes were used for analysis in this study from the four patients, all recording from primary visual cortex (Table S3). Each electrode was a platinum plate, either 2.3-mm or 1.15 mm in diameter (exposed recording area) with center-to-center spacing of 4-10 mm between adjacent electrodes on the grid or strip. The electrode positions were identified on post-operative computed tomography (CT) images. The CT images were aligned with the preoperative anatomical MRIs. We compensated for discrepancies between the two types of brain images caused by shifts in brain structure from electrode implantation using a method described in (Hermes et al., 2010). When compared to ground truth, as established by intrasurgical photography of exposed electrodes, this method has an average error of 2.6 mm (distance between location computed by alignment and location measured by photography).

Anatomical and Functional MRI

MRI sessions were conducted to localize visual field maps and electrode positions. The MRI session took place prior to electrode implantation. In two subjects, we acquired both functional and anatomical MRI (S1 and S3). For S2 and S4, we acquired only anatomical MRI, and derived retinotopic maps from the subject's individual anatomy using a published retinotopic template (Benson et al., 2014; Benson et al., 2012).

The procedures for MRI acquisition have been described previously (Winawer et al., 2013), and are briefly summarized here. The MRI sessions took place at the Center for Neurobiological Imaging (CNI) or the Lucas Center, both at Stanford University using a GE 3T scanner. We acquired T1-weighted anatomical scans (3D SPGR) of the whole brain at 1-mm resolution. The T1-weighted images were segmented into gray/white voxels using FreeSurfer's autosegmentation algorithm (http://surfer.nmr.mgh.harvard.edu/ (Dale et al., 1999)). Functional MRI scans were acquired as echo planar images using gradient echo. In addition, a separate T1-weighted anatomical scan was acquired in conjunction with fMRI scans that matched the slice prescription of the functional scans. This 'inplane' anatomical scan was used to co-register the functional images with the whole-brain T1 image. Visual field maps were identified based on fMRI data as described in previous work (Winawer et al., 2010). The field of view for fMRI was 192 x 160 mm, with 2.5 mm isotopic voxels (TR = 1.5 s, TE = 29 ms). Data were pre-processed via field map correction, slice time correction, motion compensation, and then projected from the EPI space to the whole brain anatomy, as described previously (Winawer et al., 2010; Winawer et al., 2013). Both pre-processing and pRF analysis code are part of the in-house written, freely available vistasoft toolbox (https://github.com/vistalab/vistasoft). Because data were not averaged across subjects, all analysis took place in the native space of the individual subjects.

Localization of primary visual cortex

To verify that each of the electrodes under study was located in V1, two methods were used. First, a V1-V3 atlas was applied to the T1-weighted whole brain anatomy, using publicly available software (https://hub.docker.com/r/nben/occipital_atlas/), based on work by Noah Benson and colleagues (Benson et al., 2014; Benson et al., 2012). Using the Benson atlas, it is clear that the electrode positions are in V1 and not V2 (Figure 1A). Second, a V1 probabilistic atlas was derived from the same T1-weighted anatomy using Freesurfer (http://freesurfer.net/). The files used for this are called 'lh.v1.prob' and 'rh.v1.prob', and are produced by the *recon-all* command. This probabilistic atlas was created by Hinds et al (Hinds et al., 2008). They used MRI based anatomical alignment tools (FreeSurfer) combined with high resolution imaging of ex vivo brains. They were able to define the full extent of V1 based on the Stria of Genari, enabling the probabilistic atlas to extend from the central fovea to the far periphery. We applied this probabilistic atlas to all of our subjects and show that all of our 5 electrodes are located in high probability regions of V1 (Figure 1B).

Electrophysiological Recording and Artifact Rejection

We recorded signals with a 128-channel recording system made by Tucker Davis Technologies (http://www.tdt.com/). Off-line, data were re-referenced to the common average, excluding channels with large artifacts or epileptic activity, as determined by the patient's neurologist (author JP).

Stimuli for ECoG experiments

Display. Methods for ECoG visual field mapping experiments were reported previously in detail (Winawer et al., 2013). Here we summarize the methods and note a few differences. ECoG data for S3 comprise a subset of those published in (Winawer et al., 2013), and were re-analyzed here. Experiments were conducted in the subject's hospital room using a 15-inch MacBook Pro (S3) or a 13-inch MacBook Air (S1, S2, S4) for stimulus presentation, placed at a distance to the subject close enough to ensure a sufficient field of view to map the receptive fields of pre-selected electrodes, based on the electrode anatomical location (range: 30 cm – 61 cm), with the center of the screen at eye level. If the electrode was over an anterior part of V1, then its receptive field was assumed to be peripheral, and a closer viewing distance was needed. All stimuli were confined to a circular aperture whose diameter was equal to the screen height, corresponding to a visual angle of 19.2 – 32.9 deg. For S1, the fixation dot was on the left side of the screen, rather than

in the center, in order to maximize the field of view in the right hemifield because the electrode of interest (site 1) was anterior with a very peripheral receptive field. The display had a resolution of 1440 x 900 pixels and a nominal refresh rate of 60 Hz. The refresh rate was measured by the PsychToolbox function 'FrameRate'. The frequency of the square-wave patterns (see below) was adjusted slightly to be an integer multiple of the measured refresh rate (7.466 Hz rather than 7.5 Hz). Display luminance was measured with a Minolta Color Meter II in the patient rooms to quantify image contrast. Minimum and maximum luminance were approximately 24.6 and 203 cd/m^2 for S1, S2, and S4, and 2.4 and 24.7 cd/m^2 for S3, who requested reduced screen and room illumination for comfort.

The moving bar stimuli were identical to those used previously for fMRI experiments (Amano et al., 2009; Dumoulin and Wandell, 2008; Winawer et al., 2010). A contrast pattern was viewed through a bar aperture that swept across the visual field in 12 1-second steps. There were 8 sweeps across the visual field, including 4 cardinal directions (left to right, right to left, top to bottom, and bottom to top) interspersed with four diagonals (see Figure 3 for the sequence). The cardinal sweeps consisted of 12 discrete steps whereas the diagonals sweeps consisted of 6 steps (from the screen corner to the screen middle) followed by a 6-second blank (zero-contrast, mean luminance); the blanks help to estimate the baseline response level. For all subjects, the bar width was 1/8 the maximum bar height.

The contrast of the checkerboard pattern within the moving bars was the maximum afforded by the display given the ambient illumination in the hospital room (78%-82%).

Fixation task. During the experiments, participants viewed a small central fixation dot, which alternated between red and green at random intervals (average once per 3 s). Participants pressed a button on an external number pad to indicate a change in fixation color. The purpose of the fixation task was to ensure central fixation. All participants responded to the fixation color changes with high accuracy.
Visual stimuli were generated on a Macintosh MacBook Pro in the Matlab programming environment using in-house software, made freely available (http://vistalab.stanford.edu/software/). The software tools are built on functions from the PsychToolbox (Brainard, 1997; Pelli, 1997).

PRF model fitting
The pRF models were computed as described previously, using a 'Compressive Spatial Summation' variant of the linear pRF model , of the form,

$$r(t) = g \times \left(\int S(x,y,t)\, P(x,y) dx dy \right)^n$$
$$P(x,y) = e^{-\frac{(x-x_0)^2+(y-y_0)^2}{2\sigma^2}} \qquad \text{(Eq S1)}$$

where the pRF is *P()*, the receptive field center is (x_0, y_0), the amplitude is scaled by gain factor *(g)*, and the apparent receptive field is $\sigma/\sqrt{n}$, which corresponds to the receptive field of the response when the stimulus is a point.

In this model, the stimulus *(S)* is represented as a series of 2D contrast images, the spatial receptive field *(P)* is represented as a 2D circularly symmetric Gaussian, and a static nonlinearity (*n*; power-law function) is applied to the output. When the power-law exponent is one, the model is linear, like the pRF model introduced for fMRI measurements by Dumoulin and Wandell . When the exponent is less than one, the model predicts compressive (subadditive) spatial summation. The CSS model was developed to account for a range of fMRI data in visual cortex .

As in our previous work , the output nonlinearity, *n*, was a free parameter for the broadband models, and was forced to be exactly 1 for the stimulus-locked model. Hence the stimulus-locked model was linear, and the broadband model was not.
The pRF models were fit to each of the 5 electrode's broadband and stimulus-locked time series separately (5x2 models) by minimizing the difference between the predicted response and the observed response, according to a least squares metric using nonlinear optimization (MATLAB Optimization Toolbox). Before fitting the model, data were preprocessed and averaged across repeated experiments with the identical stimulus..

The models were seeded with a Gaussian centered at the image center, *sigma* equal to the maximum stimulus extent, and n=1. To reduce the chance of finding a local minimum, the model was solved stepwise. In the first iteration, *n* was fixed at 1 and the x,y, sigma, and gain parameters were optimized. In the second iteration, applied only to the broadband data, *n* was allowed to vary.

The code to solve the pRFs is included in our repository. The wrapper function is *ebs_solve_PRF_models.m*.

Stimuli for fMRI experiments
Stimuli were presented using a Samsung SyncMaster 305T LCD monitor positioned at the head of the scanner bed. Subjects viewed the monitor via a mirror mounted on the RF coil. The monitor operated at a resolution of 1280 x 800 at 60 Hz, and the luminance response of the monitor was linearized using a lookup table based on spectrophotometer measurements. The minimum and maximum luminance was 1.4 cd/m^2 and 121 cd/m^2, respectively. Stimuli subtended 12.5–12.8° of visual angle. A button box recorded behavioral responses.

The bar stimuli used in fMRI experiments were the same as those used in ECoG experiments except for two differences: the duration of each aperture position was 1.5 s rather than 1 s; the number of discrete steps in one sweep of the visual field was 16 rather than 12; the contrast pattern within the aperture drifted rather than flickered (2 Hz temporal frequency) (see (Dumoulin and Wandell, 2008) and (Winawer et al., 2010)). Between 2 and 4 fMRI bar scans were conducted, and the time series were averaged from repeated scans prior to further analysis. The fixation task was identical to the ECoG fixation task.

Broadband and Stimulus-locked ECoG Responses

The time series of the broadband and stimulus-locked responses to bar stimuli were constructed by short-time Fourier analysis. The window for Fourier analysis was the duration that a stimulus aperture remained in a position (1 second). The time series from the one-second window was multiplied by a Hann window (raised cosine) to reduce edge artifacts.

For the broadband data, a line was fit in log-log space to the signal power (squared amplitude) of Fourier components from 8 Hz to 150 Hz, excluding values within 2 Hz of even harmonics of the stimulus frequency (15, 30, 45, 60, 75, 90, 115, 120, 135, and 150 Hz). The slope of the line was forced to be the same for all stimulus positions for a given electrode. The height of the line at 30 Hz was taken as the broadband signal for that time point.

Because the stimulus contrast reversed 15 times per second, a stimulus locked signal is found at multiples of 15 Hz (Figure 1). Of these harmonics, we found that the response at 30 Hz was most reliable, and we defined the stimulus-locked as the amplitude at 30 Hz, after subtracting the broadband fit. In previous work, we defined the stimulus locked response as the amplitude at 15 Hz for the same stimulus (Winawer et al., 2013). The reason we chose 30 Hz here is that the response at 15 Hz can be obscured by non stimulus-locked oscillations near this frequency (alpha oscillations). The pattern of results in terms of overlap between pRFs and EBS phosphenes was the same whether we defined the stimulus-locked signal as the amplitude at 15 Hz, 30 Hz, or the sum of the two, but 30 Hz yielded pRF models which explained highest variance in the time series.

As in our previous work (Winawer et al., 2013) , spectral power was used to measure the broadband response. We use power rather than amplitude because when the temporal frequency phases are random signal superposition is additive with respect to power. Specifically, if the phases are random the sum of the power spectrum of signal X and the power spectrum of signal Y is on average the power spectrum of signals X + Y. Amplitude was used as the dependent measure for the stimulus-locked signal because the phase of the response at stimulus harmonics (e.g., 30 Hz) were roughly constant across trials; if the phase is constant, amplitude rather than power is additive.

Electrical Brain Stimulation

Electrical brain stimulation is a safe procedure used routinely in clinical neurology practice. Electrical biphasic and rectangular pulses were delivered at different frequency, pulse width, amplitude, and durations (Table S2). These pulses were current-regulated and charge balanced (i.e., no charge accumulation with toxic effect on the tissue). For each site, one electrode was in V1 and the other channel was in a non-visually responsive region, remote from V1. Occasional sham trials were intermixed with stimulation trials. The subjects were not informed which trials were sham and which contained stimulation. The neurologist (author JP) was aware of the stimulation conditions, so the study was single blind rather than double blind. EBS trials took place 1-2 days after ECoG visual mapping experiments. In each experiment, the charge density per pulse was kept within the recommended limits (~50 µC/ pulse, see Table S2 for more information about EBS safety). In our analysis, we relied on the accumulated charge during a stimulus trial rather than the analysis of charge density per pulse because we noticed that subjects' rating of phosphenes not only depended on the amplitude and width of single pulses but also their frequency (i.e., the total number of pulses delivered per unit of time). Calculations of stimulation parameters were as follows: *Electrical charge* = time (s) * current (A); *Charge per pulse (µC)* = pulse width (ms) * current (mA); *Charge density per pulse (µC/cm^2 per pulse)* = charge per pulse/ electrode surface area (cm^2), Electrode surface area (cm^2)= πr^2 (3.14 * (0.2 or 0.1cm)^2 = 0.126 cm^2 or 0.063 cm^2; *Pulses per stimulation trial* = frequency (Hz) * duration (s); *Charge per trial (µC)* = charge per pulse (µC) * pulses per stimulation trial.

Electrical brain stimulation in patients with implanted electrodes is applied routinely for the purpose of functional mapping with great safety profile. The limit of ~50*µC/cm^2/pulse* was chosen as a guide based on our reading of the recent literature, but we are mindful that the current guidelines were established on the basis of studies of *continuous* electrical stimulations i.e., for hours or days of non-stop electrical charge delivery (Agnew et al., 1983; Babb and Kupfer, 1984). EBS is often applied to a small region of the brain in patients with Parkinson disease continuously with frequencies in the range of 200-300 electrical pulses per second for years without harmful effects.

Phosphene recordings

During the EBS sessions, subjects viewed the same laptop used for the ECoG visual mapping experiments, viewed from the same distance. The screen was blank other than a polar grid (Figure 3b). Subjects were instructed to fixate the center of the grid prior to EBS, and to draw the outline of their visual percept on the screen using the laptop touchpad immediately following stimulation. The purpose of the polar grid was to provide a spatial reference so that the subjects could accurately encode and then reproduce the location of the phosphene. Immediately after the subject drew the phosphene outline, we recorded the image via screen capture. Offline, the phosphene images were loaded into Matlab, and digitized by marking approximately 20 points along the phosphene outline (Figure S3).

On a few trials, the subject reported seeing two distinct phosphenes, approximately symmetric above and below the horizontal midline, and drew the outline of both. One was always much larger than the other. We interpreted this as charge spreading across the

banks of the calcarine sulcus, as the dorsal and ventral banks are close together and represent approximately symmetric positions in the visual field. On these trials, we analyzed only the larger phosphene.

Subjective ratings

Subjective ratings of phosphene intensity were obtained immediately after drawing the phosphene outline for sites 2, 3, and 5 (and not for sites 1 and 4). For site 3 and 5 (S3), the subject was instructed to indicate on a scale from 1-10 how much motion, color, and brightness was in each phosphene. Specifically, the instructions were one of three questions, '*Was it colorful?*', '*Did it move?*', or '*Was it bright?*', followed by '*Please give a number from zero to ten, zero being the least, ten being the most.*' It appeared that the subject did not use the ratings independently, as the three ratings were almost always the same for a given phosphene. Hence we collapsed the three ratings per trial into one (using the median if the three were not identical). For S2, whose experiment took place later, we asked for only a single rating of 1-10 to indicate the intensity of the percept. For this subject, we asked, '*How intense was it? Please give a number from zero to ten, zero being the least, ten being the most.*'

For some trials, the subject offered a spontaneous description. Descriptions of phosphene appearance could not be quantified and were not produced on every trial, so we do not report them in the results. Some examples are below. See Table S2 for stimulation parameters on these trials.

- Site 5, trial 2: It had the illusion of motion, but went nowhere unless I move my eyes.
- Site 5, trial 3 (phosphene seen but no drawing): Very faint dot right here. [In response to, 'Did it move?':] All look like they are moving, but it wasn't moving.
- Site 5, trial 4: Lots of splattering and flickering
- Site 5, trial 6 (sham): Nothing.
- Site 5, trial 9: Oh wow! I think that one might have left an afterimage for a second. It was loud and noisy.
- Site 5, trial 10 (sham): Nothing.
- Site 5, trial 11: I saw that here- was a 3 in color. I guess a 3 in motion and Brightness- a 3. It was one of those wimpy ones. If I was driving down the street I might be able to see that. The one before it I would have to pull over.
- Site 5, trial 17: Looks like someone is having a party and opens the windows for a second.
- Site 3, trial 9 (no drawing): Can barely make them out. I'm not sure where they are, but they were very faint. But I definitely saw them.

Computation of phosphene cortical area

Phosphenes were projected to the surface of V1 based on the subject's retinotopic map in order to infer the area of activated cortex resulting from EBS. The projection was defined as the set of voxels in V1 whose retinotopic coordinates (x,y) were within the polygon defined by the digitized phosphene. These voxels formed a region of interest, and the surface area of this region of interest was computed on the 3D cortical manifold using methods described previously (Dougherty et al., 2003). The Matlab function used for this computation is 'roiSurfaceArea', part of the freely available in-house vistasoft software (https://github.com/vistalab/vistasoft).

The calculations above have the advantage of relying on the individual subject's retinotopic maps, thereby respecting individual differences in the size and cortical magnification of V1. To confirm that these methods gave reasonable results, we also computed the surface area using a standard formula for cortical magnification (Horton and Hoyt, 1991) . For this calculation, we found the eccentricity of the centroid of the digitized phosphene and then multiplied the area of the phosphene by the cortical magnification according to the formula, $M_{area} = 300/(E + 0.75)^2$, where M is the cortical magnification and E is the eccentricity (Horton and Hoyt, 1991) . The two calculations of surface area were very highly correlated (R^2 = 0.994, 0.980, 0.996, 0.968, 0.966 for sites 1-5), with some variability in slope (0.986, 0.680, 0.658, 1.100, 0.737) when plotting the surface area from the formula as a function of the surface area computed from the individual subject data. A slope of <1 indicates that the standard formula underestimates the area relative to the area from the individual subject map.

Because the surface area of the individual subject is based on a discrete list of cortical nodes (those whose pRF center was within the phosphene drawn by the subject), this estimate could be inaccurate for small phosphenes. In particular, for small phosphenes sometimes there were 0 vertices with pRFs inside the phosphenes. On the other hand, the surface area computed from the standard formula for cortical magnification is continuous and can therefore estimate arbitrarily small cortical areas. In order to respect individual differences in cortical magnification, while at the same time avoiding the pitfalls of computing surface area based on a discrete list of cortical nodes, we derived surface areas by predicting the individually fit values from the standard formula for each subject.

Statistics and model fitting

Overlap coefficients. Overlap between phosphenes outlined by the subjects and the pRFs measured by ECoG was summarized by the Sørensen-Dice coefficient, where the overlap coefficient, O, between region A and region B is 2 times the area of overlap divided by the sum of the two areas:

$$O(A,B) = 2 \times \left[\frac{area\ (A \cap B)}{area(A) + area(B)} \right] \qquad \text{(Eq S2)}$$

For pRFs, the area was defined as the region within 2 standard deviations of the center. For each site and on each trial, two Sørensen-Dice coefficients were computed, one between the broadband pRF and the phosphene, and one between the stimulus-locked pRF and the phosphene. To assess whether the coefficients from the broadband pRFs differed significantly from the coefficients from the stimulus-locked pRFs for a given site, a bootstrapping procedure was used: for *n* paired coefficients (18, 21, 16, 18 or 9 for sites 1-5), *n* pairs were drawn at random with replacement, 10,000 times. For each of the 10,000 bootstraps, the mean of the *n* differences was computed. The fraction of these *n* differences greater than 0, 'μ', is used to derive a 2-sided *p-value*:

$$p_{value} = 1 - 2 \times \mathrm{abs}(0.5 - \mu) \qquad \text{(Eq S3)}$$

A bootstrapping test was used rather than parametric statistics because there is no assumption that the data are normally distributed. Both the *p-value* and the fraction μ are reported in Table S3.

PRF fits. PRF models were fit to the broadband and stimulus-locked time series using nonlinear optimization, as described previously (Winawer et al., 2013). The accuracy of the pRF models fit to each of the 5 sites for each of the two signals (broadband and stimulus-locked) was computed as the coefficient of determination (Table S3), as previously (Kay et al., 2013):

$$R^2 = 100 \times \left[1 - \frac{\sum(MODEL - DATA)^2}{\sum DATA^2}\right] \qquad \text{(Eq S4)}$$

Effects of stimulation parameters. The effects of charge deposited per trial on the size of phosphenes in visual space, on the size of phosphenes projected to the cortex, and on subjective numerical ratings, were summarized by the best fitting power function of the form $y=b*x^m$ (Figure 4A-D). The fits were obtained in Matlab using the function 'fit.m', using the method of nonlinear least squares. The parameters of the fits and goodness of fit values are reported in Table S4. For modeling the cortical area of phosphenes and subjective rating linear regression was computed using the Matlab function 'fitlm.m', with the parameters plotted in Figure S4.

Data Availability

In the interest of reproducible computation in neuroscience, the full set of Matlab code and data needed to reproduce all plots and analyses will be made publicly available via the Open Science Framework (https://osf.io/pz42u/, DOI 10.17605/OSF.IO/PZ42U).

Supplemental References

Agnew, W.F., Yuen, T.G., and McCreery, D.B. (1983). Morphologic changes after prolonged electrical stimulation of the cat's cortex at defined charge densities. Exp Neurol 79, 397-411.

Amano, K., Wandell, B.A., and Dumoulin, S.O. (2009). Visual field maps, population receptive field sizes, and visual field coverage in the human MT+ complex. Journal of neurophysiology 102, 2704-2718.

Babb, T.L., and Kupfer, W. (1984). Phagocytic and metabolic reactions to intracerebral electrical stimulation of rat brain. Exp Neurol 86, 183-197.

Benson, N.C., Butt, O.H., Brainard, D.H., and Aguirre, G.K. (2014). Correction of distortion in flattened representations of the cortical surface allows prediction of V1-V3 functional organization from anatomy. PLoS Comput Biol 10, e1003538.

Benson, N.C., Butt, O.H., Datta, R., Radoeva, P.D., Brainard, D.H., and Aguirre, G.K. (2012). The retinotopic organization of striate cortex is well predicted by surface topology. Curr Biol 22, 2081-2085.

Brainard, D.H. (1997). The Psychophysics Toolbox. Spat Vis 10, 433-436.

Dale, A.M., Fischl, B., and Sereno, M.I. (1999). Cortical surface-based analysis. I. Segmentation and surface reconstruction. Neuroimage 9, 179-194.

Dougherty, R.F., Koch, V.M., Brewer, A.A., Fischer, B., Modersitzki, J., and Wandell, B.A. (2003). Visual field representations and locations of visual areas V1/2/3 in human visual cortex. J Vis 3, 586-598.

Dumoulin, S.O., and Wandell, B.A. (2008). Population receptive field estimates in human visual cortex. Neuroimage 39, 647-660.

Hermes, D., Miller, K.J., Noordmans, H.J., Vansteensel, M.J., and Ramsey, N.F. (2010). Automated electrocorticographic electrode localization on individually rendered brain surfaces. Journal of neuroscience methods 185, 293-298.

Hinds, O.P., Rajendran, N., Polimeni, J.R., Augustinack, J.C., Wiggins, G., Wald, L.L., Diana Rosas, H., Potthast, A., Schwartz, E.L., and Fischl, B. (2008). Accurate prediction of V1 location from cortical folds in a surface coordinate system. Neuroimage 39, 1585-1599.

Horton, J.C., and Hoyt, W.F. (1991). The representation of the visual field in human striate cortex. A revision of the classic Holmes map. Archives of ophthalmology 109, 816-824.

Kay, K.N., Winawer, J., Mezer, A., and Wandell, B.A. (2013). Compressive spatial summation in human visual cortex. Journal of neurophysiology 110, 481-494.

Pelli, D.G. (1997). The VideoToolbox software for visual psychophysics: transforming numbers into movies. Spat Vis 10, 437-442.

Winawer, J., Horiguchi, H., Sayres, R.A., Amano, K., and Wandell, B.A. (2010). Mapping hV4 and ventral occipital cortex: the venous eclipse. Journal of vision 10, 1.

Winawer, J., Kay, K.N., Foster, B.L., Rauschecker, A.M., Parvizi, J., and Wandell, B.A. (2013). Asynchronous broadband signals are the principal source of the BOLD response in human visual cortex. Curr Biol 23, 1145-1153.